2016-07-01

The Effects of Antenna Coupling in a MIMO Radar System

Benjamin T. Arnold
Brigham Young University

The Effects of Antenna Coupling in a MIMO Radar System

Benjamin T. Arnold

A thesis submitted to the faculty of
Brigham Young University
in partial fulfillment of the requirements for the degree of

Master of Science

Michael A. Jensen, Chair
Karl F. Warnick
David G. Long

Department of Electrical and Computer Engineering, BYU

Brigham Young University

July 2016

ABSTRACT

The Effects of Antenna Coupling in a MIMO Radar System

Benjamin T. Arnold
Department of Electrical and Computer Engineering, BYU
Master of Science

A mathematical model for a multiple-input multiple-output radar system is presented. The model is used to track signals through the system in order to identify the impact of antenna array mutual coupling on radar system performance. Simulations using the model provide quantitative assessment of the performance degradation as a function of antenna coupling strength. Specifically, the results show that coupling can cause a target to appear at an angle notably different than its actual angle and can cause an increase in the side lobe level. A compensation technique is presented that completely removes these effects for practical levels of coupling. However, it is highly sensitive to inaccurate measurements of the system as well as time-varying system components. The technique may degrade the system performance further in some cases. Matching network design techniques and their impact on the system performance are also examined. For some levels of coupling they provide marginal improvement but may decrease system performance for other levels.

Keywords: MIMO systems, radar, mutual coupling, matching network

ACKNOWLEDGMENTS

I would first like to express appreciation for my advisor Michael Jensen. He provided invaluable help and encouragement throughout this project. It was a privilege for me to work with him.

Being a committee member takes time and effort. Thank you to Karl Warnick and David Long for helping me in this capacity.

Many colleagues have influenced my work and made the journey enjoyable. I would especially like to notice Matthew Arnold, James Eck, Yaedem Gagakuma, and Jonathan Spencer.

Thank you to my wife, Tasha, for always expressing interest in my work and for believing in me. Thank you to my father, David, for being a mentor and example. Thank you to my mother, Linda, who taught me the importance of education. And thank you to my siblings, Amy, Matthew, and Jonathan, for their friendship and companionship in studying.

Table of Contents

List of Figures

Chapter 1

Introduction

Multiple-input multiple-output radar systems are well documented [1–6]. Despite all of the research that has appeared detailing the performance of multiple-input multiple-output (MIMO) radar, only one paper [7] addresses the effects of antenna mutual coupling. While this prior research demonstrates both simulated and experimental results confirming the degradation of performance due to coupling, the model for coupling used in the simulations is rudimentary and does not have a physical interpretation.

In contrast, the effects of coupling on a MIMO communication system have been researched extensively [8–16]. This research includes the study of methods for designing coupled and uncoupled matching networks to mitigate the negative effects of coupling, concepts that are useful in studying coupling in radar systems. However, the manner in which coupling affects a communication system differs from how it affects a radar system, necessitating a detailed analysis in order to quantify the impact of coupling and matching on radar system performance.

More specifically, while signal processing techniques are applied to arrays of antennas in both communication and radar systems, in communication systems these techniques are typically used on the transmit and receive arrays separately. This matches the physical coupling that exists within each array, making the analysis detailed but straightforward. In MIMO radar systems, however, the signal processing combines the transmit and receive arrays into a single virtual array to which beamforming can be applied, which means that the impact of coupling observed within each physical array must be properly represented in the virtual array signal model.

This thesis examines the effects of mutual coupling on a MIMO radar system. The work first formulates a model that connects the physical coupling to the signals that appear

on the virtual array. Simulations based on this model are then used to quantify the impact of coupling on performance in realistic environments. Two performance metrics are developed that provide simple comparative performance assessment based on the simulation results. Finally, the analysis and simulations are used to demonstrate coupling compensation and the impact of proper impedance matching on system performance.

1.1 Contributions

This thesis offers several relevant contributions:

- The work presents a detailed mathematical model for a MIMO radar system. The transmit portion of the model includes a matching network and coupled antennas. The channel contains time-varying point targets. The receive portion of the model includes coupled antennas, a matching network, and noisy amplifiers. Each aspect of the model is derived from an accurate representation and is analyzed using network theory. Thus, the model is applicable more broadly.

- The thesis provides a mathematical definition for coupled signals and for uncoupled signals. This separation enables the flexibility of comparing outputs from the radar when coupling is present in the system to those when coupling is removed from the system.

- The work details simulation results based on the model that quantify the effects of coupling on MIMO radar performance. These results are shown for two metrics that measure the ability to accurately detect the target angle and the resulting increase of the side lobe level for a target. Each metric is significantly affected for practical levels of coupling.

- The thesis describes a technique for coupling compensation and an analysis of its performance impact. For practical levels of coupling, compensation is successful and can entirely remove the effects of coupling in a known system. The shortcomings of the technique are examined. Simulated results show that the technique can be highly sensitive in normal applications.

- Finally, the work demonstrates the minimal performance improvement offered by various matching network design criteria from the literature.

1.2 Organization of Thesis

The thesis is organized as follows. Chapter 2 provides background for a MIMO radar system. The fundamentals required for understanding include orthogonality, virtual arrays, and mutual coupling. Chapter 3 provides a mathematical framework for defining a MIMO radar system. This framework, derived using network theory, includes a transmitter consisting of a matching network and coupled antennas and a receiver consisting of a matching network, coupled antennas, and noisy amplifiers. The channel contains time-varying point targets.

Chapter 4 discusses how signals travel through the radar and provides the framework for mathematically separating coupled signals and uncoupled signals. Following is an examination of how coupling impacts the ability of the radar to detect targets. The analysis includes how coupling shifts the perceived target angle and how it increases the side lobe level.

Chapter 5 describes a technique that compensates for coupling in the system. In ideal simulations the effects of coupling are entirely removed. The technique is highly sensitive to inaccurate measurements of system parameters and variations in the system that occur over time. Simulation results quantify the performance impact.

Finally, Chapter 6 discusses using matching network design techniques with different criteria borrowed from the MIMO communication literature. The affect on performance is quantified for the two metrics discussed in Chapter 4.

Chapter 2

Background

The following background material provides the fundamental concepts required to understand the developments in this thesis. It begins with a brief introduction to MIMO radar and a comparison with traditional radar. It summarizes the concept of orthogonal waveforms and presents different ways of achieving orthogonality. It also discusses the use of orthogonal waveforms to form a virtual array as well as the fundamentals of antenna mutual coupling.

2.1 MIMO Radar

Like some traditional radar systems, a MIMO radar system uses an array of transmit antennas in combination with an array of receive antennas. The distinguishing factor for a MIMO radar is that it transmits mutually orthogonal signals providing the ability to separate the signals on a given receive antenna by their transmitter origin. This is fundamental to the concept of a virtual array that will be discussed later. Beamforming on the virtual array is the signal processing technique that achieves the equivalent of beamforming on the transmit and receive arrays simultaneously. Thus, a MIMO radar system can realize beamforming for all angles on both the transmit and receive arrays from a single pulse. A traditional radar, however, requires a new pulse to be transmitted for each desired beamforming angle on the transmit array.

In general, the antennas in a MIMO radar may be placed far apart so as to increase the variation in sampling the statistical properties of a target. However, only the case of co-located antennas will be examined here, where all of the antennas are separated by a distance on the order of a wavelength. This is a common application of MIMO radar as it is difficult to know the relative positions of transmit and receive antnnas within an increment

of a wavelength when they are far apart. Antennas that are in close proximity experience mutual coupling between elements [17].

2.2 Orthogonality

In order to determine the transmitter origin of a signal that has been received in a MIMO radar, the signals transmitted must be mutually orthogonal (the signals must form an orthogonal set).

Consider two functions, f_i and f_j, from a finite set of functions. These functions are orthogonal over the region $[a, b]$ with respect to the inner product $\langle \cdot, \cdot \rangle$ when

$$\langle f_i, f_j \rangle = \int_a^b f_i(t) f_j(t) dt = 0. \tag{2.1}$$

This set of functions forms an orthogonal set when, for every combination of i and j within the set,

$$\langle f_i, f_j \rangle = \int_a^b f_i(t) f_j(t) dt = \langle f_i, f_i \rangle \delta_{i,j}, \tag{2.2}$$

where

$$\delta_{i,j} = \begin{cases} 1, & i = j \\ 0, & i \neq j \end{cases}. \tag{2.3}$$

There are many sets of functions that satisfy (2.2). Commonly, signals are separated in time or frequency. But orthogonality can also be achieved through proper modulation of the waveform.

2.2.1 Time

For time orthogonality to be achieved only one transmitter may be on at a given time [5]. This can be accomplished using a simpler architecture than any of the other methods require. However, the time to synthesize a virtual array using time-orthogonal signals is significantly longer than that for any of the other methods discussed.

A set of time orthogonal signals is mathematically defined as

$$f_i(t) = \begin{cases} f(t - iT), & iT \leq t < (i+1)T \\ 0, & \text{otherwise} \end{cases} \tag{2.4}$$

where f is an arbitrary signal and T is the duration of time that any given transmitter is on. Orthogonality can be shown by inserting (2.4) into (2.2). Figure 2.1 shows an example of two time orthogonal signals, f_0 and f_1.

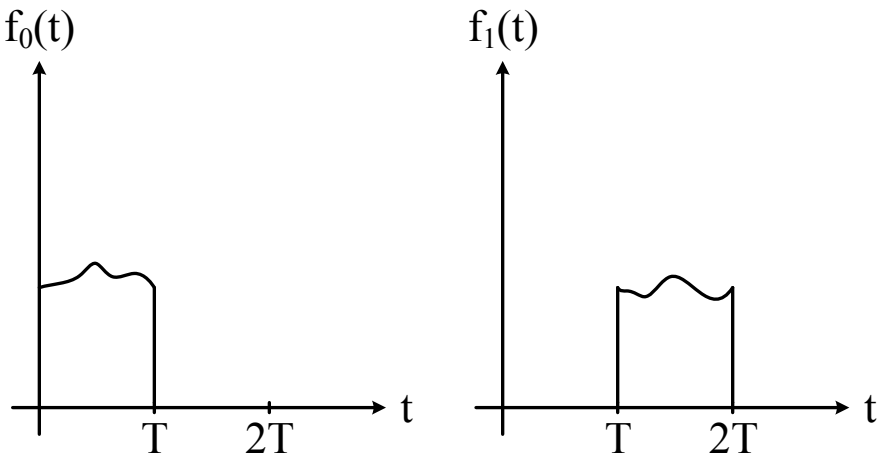

Figure 2.1: Two time orthogonal signals.

2.2.2 Frequency

Another means of generating orthogonal signals is to use chirped signals with differing frequency offsets [4]. Such a set of signals can be defined as

$$s_i(t) = e^{j2\pi(f_{c,i}t + \frac{k}{2}t^2)}, \tag{2.5}$$

where $f_{c,i}$ is the center frequency for the ith transmit signal and k is the chirp rate [5]. The instantaneous frequency is plotted for a number of example signals against time in Fig. 2.2.

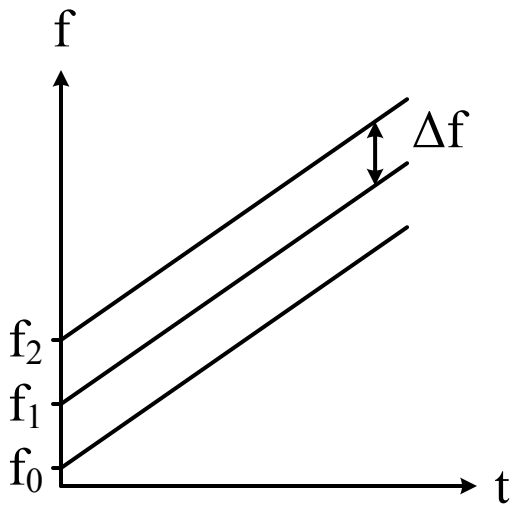

Figure 2.2: Instantaneous frequency of a set of chirped signals offset in frequency.

Using signals that are orthogonal in frequency allows all of the transmitters to be on simultaneously but requires a more complex architecture. Each receive channel requires a set of matched filters equal to the number of transmit channels. Inserting two functions, s_i and s_j, from (2.5) into (2.2) results in

$$\begin{aligned} p_{uv} &= \int_a^b e^{j2\pi(f_{\mathrm{c},u}t+\frac{k}{2}t^2)} e^{-j2\pi(f_{\mathrm{c},v}t+\frac{k}{2}t^2)} dt \\ &\approx \delta(f_{\mathrm{c},u} - f_{\mathrm{c},v}), \end{aligned} \tag{2.6}$$

where the approximation is due to the limits of integration not extending to infinity. However, this is a good approximation because the complex exponentials experience a large number of 2π phase changes over the length of integration.

The result from (2.6) suggests that the separation between the center frequencies of the chirped signals, $f_{\mathrm{c},i}$, must be large enough to remove any ambiguities caused by frequency shifts due to targets at far ranges and frequency shifts that provide orthogonality. If the center frequencies are separated by Δf then the maximum unambiguous range for a chirp rate k would be

$$R_{\mathrm{ua}} = c_0 \frac{\Delta f}{k}. \tag{2.7}$$

For a frequency separation of $\Delta f = 1$ MHz and a chirp rate of $k = 250$ GHz / sec then the unambiguous range would be $R_{\text{ua}} = 1.5$ km. Targets beyond 1.5 km correspond to a frequency shift larger than Δf causing interference with the adjacent orthogonal signals. However, this interference has very little impact because the power of the signal falls off as R^4 and will be extremely small for $R > 1.5$ km.

2.2.3 Orthogonal Waveforms

Any type of modulated orthogonal waveforms can be used. The remaining architecture following demodulation is assumed feasible and is not covered in detail here. Radar systems that require large bandwidth also require high bandwidth sampling when using this type of orthogonality technique. For this reason these types of systems are less practical and are less common.

2.2.4 Noise Analysis

Noise is added to the ith orthogonal signal s_i to produce

$$x_i(t) = s_i(t) + \nu_i(t), \tag{2.8}$$

where ν_i is zero-mean white Gaussian noise with a variance of σ_n^2, or $\nu_i \sim N(0, \sigma_n^2)$. This signal is then passed through a matched filter. Assuming chirped signals, the output of the filter for the ith signal with noise and the jth filter can be given as

$$u_{ij}(t) = s_i(t)s_j^*(t) + \underbrace{\nu_i(t)s_j^*(t)}_{n_{ij}}, \tag{2.9}$$

where n_{ij} is the term corresponding to the noise. The mean and variance of n_{ij} are computed as

$$E\{n_{ij}(t)\} = E\{\nu_i(t)\}s_j^*(t) = 0 \tag{2.10}$$

$$E\{n_{ij}(t)n_{ij}^*(t-\tau)\} = E\{\nu_i(t)\nu_i^*(t-\tau)\}s_j^*(t)s_j(t-\tau) = \sigma_n^2\delta(\tau). \tag{2.11}$$

Therefore, separating orthogonal waveforms using a matched filter does not affect the statistical properties of the noise.

2.3 Virtual Array

A virtual array is synthesized from a transmit array that transmits orthogonal waveforms and a receive array that can distinguish the orthogonal waveforms at each receive element. Each transmit-receive pair corresponds to a virtual element. Thus, there will be $N_{\mathrm{T}} \times N_{\mathrm{R}}$ virtual elements, where N_{T} is the number of elements in the transmit array and N_{R} is the number of elements in the receive array.

The position of each virtual element can be computed from its corresponding transmit and receive elements. Assuming that all elements lie in the x-y plane then the virtual element position is computed as

$$\begin{aligned} x_{\mathrm{v},ij} &= x_{\mathrm{r},i} + x_{\mathrm{t},j} \\ y_{\mathrm{v},ij} &= y_{\mathrm{r},i} + y_{\mathrm{t},j}, \end{aligned} \tag{2.12}$$

where i is the index of the receive element and j is the index of the transmit element. This transformation replicates the entire receive array at every transmit element location. The position of the replicated receive element relative to the associated transmit element is the same as the position of the original location of the receive element relative to the origin.

The equivalence of the physical arrays and the virtual array is shown through an analysis of signal propagation delays between the transmit antennas, a point target in the far field, and the receive arrays. Figure 2.3 shows a timing diagram of a system with two transmit antennas and two receive antennas. The separation between adjacent elements, d, is typically one-half wavelength. The time delay between adjacent elements receiving the signal is

$$\tau = \frac{d \cos(\theta_{\mathrm{q}})}{c_0}, \tag{2.13}$$

where θ_{q} is the angle to the target and c_0 is the speed of light in free space. The time delay, T_{ij}, from the jth transmitter to the target and back to the ith receiver is given for each of

the transmit-receive pairs for the two by two system shown in Fig. 2.3 as

$$\begin{aligned} T_{11} &= 2T_{\mathrm{q}} - \tau \\ T_{21} &= 2T_{\mathrm{q}} - 2\tau \\ T_{12} &= 2T_{\mathrm{q}} - 4\tau \\ T_{22} &= 2T_{\mathrm{q}} - 5\tau, \end{aligned} \tag{2.14}$$

where T_{q} is the time it takes for the signal to travel from the origin to the target.

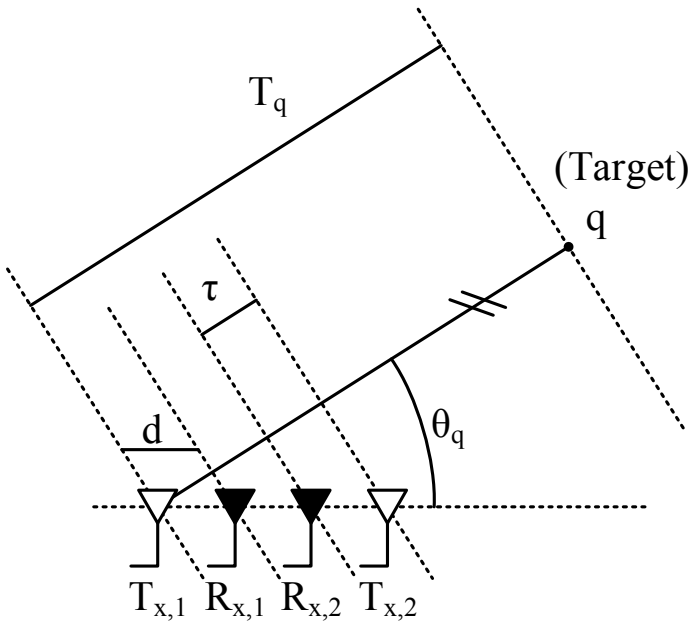

Figure 2.3: Timing for a radar system with two transmit antennas and two receive antennas.

According to (2.12) the positions of the virtual elements can be computed for the system in Fig. 2.3. The resulting positions are shown in Fig. 2.4. In order to verify that the virtual array has the same timing properties as the physical arrays a timing analysis is

done on the virtual arrays and results in

$$\begin{aligned} T_{\mathrm{V},11} &= 2T_{\mathrm{q}} - \tau \\ T_{\mathrm{V},21} &= 2T_{\mathrm{q}} - 2\tau \\ T_{\mathrm{V},12} &= 2T_{\mathrm{q}} - 4\tau \\ T_{\mathrm{V},22} &= 2T_{\mathrm{q}} - 5\tau. \end{aligned} \tag{2.15}$$

Comparing (2.15) to (2.14) shows that the timing for the virtual elements matches that for the corresponding transmit-receive pair from the physical arrays.

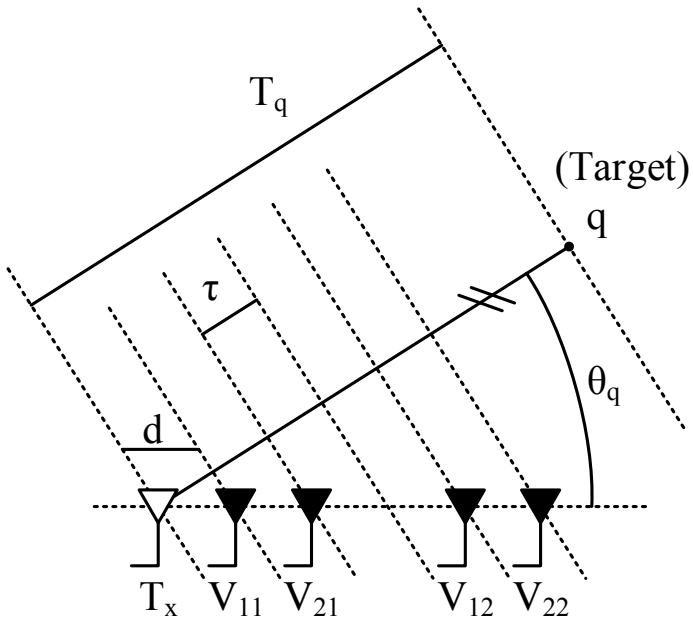

Figure 2.4: Timing for the virtual array of a radar system with two transmit antennas and two receive antennas.

The received signals associated with each virtual element, or transmit-receive pair, can be determined because the transmitted waveforms are orthogonal. Beamforming weights are computed based on the positions of the virtual elements and the desired beamforming angle. A beamforming output is produced by applying these weights to the signals corresponding

to the appropriate virtual element. Thus, beamforming is used in the same way for a virtual array as it is for a physical array.

2.4 Mutual Coupling

Mutual coupling occurs between antenna elements of an array when a current on one element induces an unintentional voltage on the nearby elements [17], [18]. This behavior is described by the impedance matrix $\mathbf{Z}$ of the array with the relationship between the terminal voltages $\mathbf{v}$ and currents $\mathbf{i}$ given as, $\mathbf{v} = \mathbf{Zi}$. The self-impedances of the antennas form the diagonal elements of $\mathbf{Z}$ and the mutual impedances are given by the off-diagonal elements of $\mathbf{Z}$ [19]. An S-parameter matrix can also be used to describe coupling and can be computed from the impedance matrix as

$$\mathbf{S} = (\mathbf{Z} + Z_0\mathbf{I})^{-1}(\mathbf{Z} - Z_0\mathbf{I}), \tag{2.16}$$

where Z_0 is the characteristic impedance and $\mathbf{I}$ is the identity matrix.

The induced voltages due to coupling generate currents when the antennas are terminated in a load. These currents then radiate and cause a distortion in the radiation pattern. This distortion has been well documented and is ignored in this study. This thesis presents how these induced currents alter the received signals and how this alteration impacts the output of the beamformer.

Chapter 3

System Model and Analysis

The MIMO radar source generates orthogonal waveforms, as discussed in section 2.2. The system model includes a mutually coupled transmit antenna array and a matching network for linking the source to the antennas. The channel models the signals propagating from the transmitter, interacting with time-varying point targets, and propagating back to the receiver. The receiver contains a mutually coupled antenna array, a matching nework that links the antennas to the receiver circuitry, noisy amplifiers, and a load termination. Network theory is used to determine the signals at the loads given a target and transmit source configuration [13]. Figure 3.1 shows a diagram of this system model. Although not shown in the system model diagram, a matched filter is then used to separate the signals on the loads by their transmitter origin in order to form the virtual array.

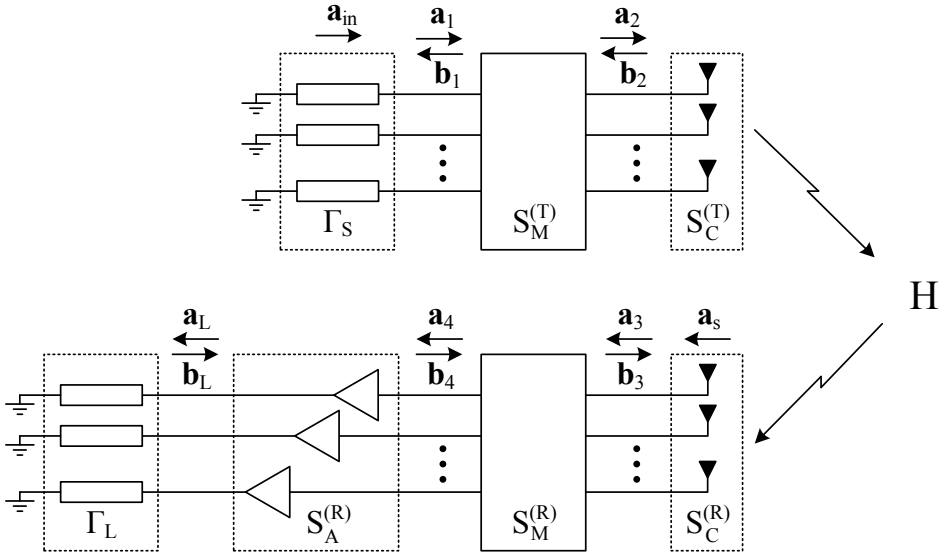

Figure 3.1: Block Diagram of the System Model.

In order to use multiplication rather than convolution, the network anaylis should be done in the frequency domain. However, it is assumed that the S-parameters and reflection coefficients are constant with frequency over the operating bandwidth of the radar. Therefore, the resulting coefficients can also be used in the time domain. In the subsequent sections the coefficients determined by network analysis in the frequency domain are combined with time domain signals.

3.1 Source

Any of the methods discussed in section 2.2 can be used to produce a set of orthogonal waveforms. We use $s_n(t)$ to denote the nth signal in this set. The vector, $\mathbf{a}_{\text{in}}$, which contains forward traveling waves from the sources is written as

$$\mathbf{a}_{\text{in}} = [s_0, s_1, \ \ldots \ , s_{N_{\text{T}}-1}]^{\text{T}}, \tag{3.1}$$

where $\{\cdot\}^{\text{T}}$ is the vector transpose.

3.2 Transmitter

The transmitter is made up of the signal source, a matching network, and an array of antennas. Given the input from the source as defined by (3.1), network theory is used to determine the currents at the inputs of the antenna array. It is assumed that the signal source has an output impedance such that its output reflection coefficient is zero. The forward traveling voltage wave at the port between the source and the matching network must then be $\mathbf{a}_1 = \mathbf{a}_{\text{in}}$.

Equations for the forward and reverse traveling waves at the port between the matching network and the antennas can be written as

$$\mathbf{a}_2 = \mathbf{S}^{(\text{T})}_{\text{M},21}\mathbf{a}_1 + \mathbf{S}^{(\text{T})}_{\text{M},22}\mathbf{b}_2 \tag{3.2a}$$

$$\mathbf{b}_2 = \mathbf{S}^{(\text{T})}_{\text{C}}\mathbf{a}_2, \tag{3.2b}$$

where $\mathbf{S}_{\mathrm{C}}^{(\mathrm{T})}$ is the S-parameter matrix for the coupled transmit antenna array and $\mathbf{S}_{\mathrm{M}}^{(\mathrm{T})}$ is the S-parameter matrix for the transmitter matching network that can be written as the block matrix

$$\mathbf{S}_{\mathrm{M}}^{(\mathrm{T})} = \begin{bmatrix} \mathbf{S}_{\mathrm{M},11}^{(\mathrm{T})} & \mathbf{S}_{\mathrm{M},12}^{(\mathrm{T})} \\ \mathbf{S}_{\mathrm{M},21}^{(\mathrm{T})} & \mathbf{S}_{\mathrm{M},22}^{(\mathrm{T})} \end{bmatrix}. \tag{3.3}$$

Substituting $\mathbf{a}_{\mathrm{in}}$ for $\mathbf{a}_1$ and solving (3.2a - 3.2b) for $\mathbf{a}_2$ results in

$$\mathbf{a}_2 = (\mathbf{I} - \mathbf{S}_{\mathrm{M},22}^{(\mathrm{T})}\mathbf{S}_{\mathrm{C}}^{(\mathrm{T})})^{-1}\mathbf{S}_{\mathrm{M},21}^{(\mathrm{T})}\mathbf{a}_{\mathrm{in}}. \tag{3.4}$$

Using that $\mathbf{b}_{\mathrm{L}} = \mathbf{S}_{\mathrm{C}}^{(\mathrm{T})}\mathbf{a}_{\mathrm{L}}$, the relationship between the currents and the forward traveling voltage waves at the port between the matching network and the antennas is

$$\mathbf{i}_2 = \frac{1}{\sqrt{Z_0}}(\mathbf{I} - \mathbf{S}_{\mathrm{C}}^{(\mathrm{T})})\mathbf{a}_2. \tag{3.5}$$

Substituting (3.4) into (3.5) gives the currents at the input port to the antennas as

$$\mathbf{i}_2 = \underbrace{\frac{1}{\sqrt{Z_0}}(\mathbf{I} - \mathbf{S}_{\mathrm{C}}^{(\mathrm{T})})(\mathbf{I} - \mathbf{S}_{\mathrm{M},22}^{(\mathrm{T})}\mathbf{S}_{\mathrm{C}}^{(\mathrm{T})})^{-1}\mathbf{S}_{\mathrm{M},21}^{(\mathrm{T})}}_{\mathbf{D}_{\mathrm{T}}}\mathbf{a}_{\mathrm{in}}, \tag{3.6}$$

where $\mathbf{D}_{\mathrm{T}}$ is a linear operator that converts input voltages from the source to currents feeding the antennas.

3.3 Channel

The channel consists of time-varying point targets. Propagating waves from the transmit array interact with these targets and return to the receiver. The currents defined by (3.6) drive the transmit antenna array and produce an electric field in the channel. This electric field is determined for the angle ϕ from the origin as

$$\widetilde{e}_{\mathrm{T}}(\phi) = \sum_{m=1}^{N_{\mathrm{T}}}\sum_{n=1}^{N_{\mathrm{T}}} e_{\mathrm{T},m}(\phi)D_{\mathrm{T},mn}a_{\mathrm{in},n}, \tag{3.7}$$

where $e_{\mathrm{T},m}$ is the radiation pattern for the mth transmit element when excited by a unit driving current and all other elements are terminated in an open-circuit [19]. After propagating through the channel the electric field at the ℓth receive antenna is computed as

$$\widetilde{e}_{\mathrm{R},\ell} = \sum_{q=1}^{N_{\mathrm{Q}}} \sum_{m=1}^{N_{\mathrm{T}}} \sum_{n=1}^{N_{\mathrm{T}}} H_{\ell qm}\{e_{\mathrm{T},m}(\theta_q) D_{\mathrm{T},mn} a_{\mathrm{in},n}\}, \tag{3.8}$$

where N_{Q} is the number of targets in the channel and θ_q is the angle to the qth target. $H_{\ell qm}\{\cdot\}$ is an operator that emulates the effect of the channel on its argument and is defined as

$$H_{\ell qm}\{f(t)\} = A_q f(t - T_{\ell qm}), \tag{3.9}$$

where A_q is the complex reflection coefficient of the qth target and $T_{\ell qm}$ is the propagation time from the mth transmit antenna to the qth target and back to the ℓth receive antenna.

The open-circuit voltage at the input port of the ℓth receive antenna is computed as

$$v_{\mathrm{oc},\ell} = \sum_{q=1}^{N_{\mathrm{Q}}} \sum_{m=1}^{N_{\mathrm{T}}} \sum_{n=1}^{N_{\mathrm{T}}} e_{\mathrm{R},\ell}(\theta_q) H_{\ell qm}\{e_{\mathrm{T},m}(\theta_q) D_{\mathrm{T},mn} a_{\mathrm{in},n}\}, \tag{3.10}$$

where the subscript $\{\cdot\}_{\mathrm{oc}}$ signifies open-circuit and $e_{\mathrm{R},\ell}$ is the radiation pattern for the ℓth receive element. When the receive antennas are terminated in open-circuits the relationship between the forward and reverse traveling voltage waves becomes $\mathbf{a}_{\mathrm{oc}} = \mathbf{b}_{\mathrm{oc}}$. The open-circuit voltage is then related to the open-circuit forward traveling voltage wave as

$$\mathbf{v}_{\mathrm{oc}} = 2\sqrt{Z_0}\mathbf{a}_{\mathrm{oc}}. \tag{3.11}$$

The antennas act as a source and generate the voltage wave $\mathbf{a}_{\mathrm{s}}$. The relationship between $\mathbf{a}_{\mathrm{s}}$ and the open-circuit voltage wave at the port of the antennas is determined by network theory as

$$\mathbf{a}_{\mathrm{s}} = (\mathbf{I} - \mathbf{S}_{\mathrm{C}}^{(\mathrm{R})})\mathbf{a}_{\mathrm{oc}}, \tag{3.12}$$

where $\mathbf{S}_{\mathrm{C}}^{(\mathrm{R})}$ is the S-parameter matrix for the coupled receive antenna array. Solving (3.11) for $\mathbf{a}_{\mathrm{oc}}$ and substituting the result into (3.15) gives

$$\mathbf{a}_{\mathrm{s}} = \frac{1}{2\sqrt{Z_0}}(\mathbf{I} - \mathbf{S}_{\mathrm{C}}^{(\mathrm{R})})\mathbf{v}_{\mathrm{oc}}. \tag{3.13}$$

3.4 Receiver with Noisy Amplifiers

The receiver model includes a coupled antenna array, a matching network, and noisy amplifiers. Network theory is used to analyze the signals in the receiver from the system model in Fig. 3.1. The voltage waves at the port between the antennas and the matching network can be written as

$$\mathbf{a}_3 = \mathbf{a}_{\mathrm{s}} + \mathbf{S}_{\mathrm{C}}^{(\mathrm{R})}\mathbf{b}_3 \tag{3.14a}$$

$$\mathbf{b}_3 = \mathbf{S}_{\mathrm{M},11}^{(\mathrm{R})}\mathbf{a}_3 + \mathbf{S}_{\mathrm{M},12}^{(\mathrm{R})}\mathbf{b}_4. \tag{3.14b}$$

Eliminating $\mathbf{b}_3$ from these expressions gives

$$\mathbf{a}_3 = \underbrace{(\mathbf{I} - \mathbf{S}_{\mathrm{C}}^{(\mathrm{R})}\mathbf{S}_{\mathrm{M},11}^{(\mathrm{R})})}_{\mathbf{A}}{}^{-1}(\mathbf{a}_{\mathrm{s}} + \mathbf{S}_{\mathrm{C}}^{(\mathrm{R})}\mathbf{S}_{\mathrm{M},12}^{(\mathrm{R})}\mathbf{b}_4). \tag{3.15}$$

The amplifiers inject both forward and reverse traveling noise waves at each amplifier input [20]. Each noise signal is modeled as an i.i.d. white Gaussian stochastic process. At the port between the matching network and the amplifiers, the equations for the voltages can be written as

$$\mathbf{a}_4 = \mathbf{S}_{\mathrm{M},22}^{(\mathrm{R})}\mathbf{b}_4 + \mathbf{S}_{\mathrm{M},21}^{(\mathrm{R})}\mathbf{a}_3 \tag{3.16a}$$

$$\mathbf{b}_4 = \mathbf{S}_{\mathrm{A},11}^{(\mathrm{R})}\mathbf{a}_4 + \mathbf{S}_{\mathrm{A},12}^{(\mathrm{R})}\mathbf{b}_{\mathrm{L}} + \mathbf{b}_{\eta}, \tag{3.16b}$$

where $\mathbf{b}_\eta$ is the reverse traveling noise signal. Equations (3.15), (3.16a), and (3.16b) are solved to eliminate $\mathbf{a}_3$ and $\mathbf{b}_4$, leading to

$$\mathbf{a}_4 = \underbrace{(\mathbf{I} - \mathbf{S}^{(\mathrm{R})}_{\mathrm{M},22}\mathbf{S}^{(\mathrm{R})}_{\mathrm{A},11} - \mathbf{S}^{(\mathrm{R})}_{\mathrm{M},21}\mathbf{A}\mathbf{S}^{(\mathrm{R})}_{\mathrm{C}}\mathbf{S}^{(\mathrm{R})}_{\mathrm{M},12}\mathbf{S}^{(\mathrm{R})}_{\mathrm{A},11})^{-1}}_{\mathbf{B}_1}[\mathbf{S}^{(\mathrm{R})}_{\mathrm{M},21}\mathbf{A}\mathbf{a}_\mathrm{s} + \underbrace{(\mathbf{S}^{(\mathrm{R})}_{\mathrm{M},22}\mathbf{S}^{(\mathrm{R})}_{\mathrm{A},12} + \mathbf{S}^{(\mathrm{R})}_{\mathrm{M},21}\mathbf{A}\mathbf{S}^{(\mathrm{R})}_{\mathrm{C}}\mathbf{S}^{(\mathrm{R})}_{\mathrm{M},12}\mathbf{S}^{(\mathrm{R})}_{\mathrm{A},12})}_{\mathbf{B}_2}\mathbf{b}_\mathrm{L} + \underbrace{(\mathbf{S}^{(\mathrm{R})}_{\mathrm{M},22} + \mathbf{S}^{(\mathrm{R})}_{\mathrm{M},21}\mathbf{A}\mathbf{S}^{(\mathrm{R})}_{\mathrm{C}}\mathbf{S}^{(\mathrm{R})}_{\mathrm{M},12})}_{\mathbf{B}_3}\mathbf{b}_\eta]. \quad (3.17)$$

Finally, at the port between the loads and the amplifiers, the equations for the voltages can be written as

$$\mathbf{a}_\mathrm{L} = \mathbf{S}^{(\mathrm{R})}_{\mathrm{A},22}\mathbf{b}_\mathrm{L} + \mathbf{S}^{(\mathrm{R})}_{\mathrm{A},21}\mathbf{a}_4 + \mathbf{a}_\eta \quad (3.18a)$$

$$\mathbf{b}_\mathrm{L} = \mathbf{\Gamma}_\mathrm{L}\mathbf{a}_\mathrm{L}, \quad (3.18b)$$

where $\mathbf{a}_\eta$ is the forward traveling noise signal and Γ_L is the reflection coefficient of the load. Equations (3.17), (3.18a), and (3.18b) are solved to eliminate $\mathbf{a}_4$ and $\mathbf{b}_\mathrm{L}$, resulting in

$$\mathbf{a}_\mathrm{L} = \underbrace{(\mathbf{I} - \mathbf{S}^{(\mathrm{R})}_{\mathrm{A},22}\mathbf{\Gamma}_\mathrm{L} - \mathbf{S}^{(\mathrm{R})}_{\mathrm{A},21}\mathbf{B}_1\mathbf{B}_2\mathbf{\Gamma}_\mathrm{L})^{-1}}_{\mathbf{C}_1}[\underbrace{\mathbf{S}^{(\mathrm{R})}_{\mathrm{A},21}\mathbf{B}_1\mathbf{S}^{(\mathrm{R})}_{\mathrm{M},21}\mathbf{A}}_{\mathbf{C}_2}\mathbf{a}_\mathrm{s} + \underbrace{\mathbf{S}^{(\mathrm{R})}_{\mathrm{A},21}\mathbf{B}_1\mathbf{B}_3}_{\mathbf{C}_3}\mathbf{b}_\eta + \mathbf{a}_\eta]. \quad (3.19)$$

This forward traveling voltage wave is related to the voltage on the loads by

$$\mathbf{v}_\mathrm{L} = \sqrt{Z_0}(\mathbf{a}_\mathrm{L} + \mathbf{b}_\mathrm{L}) = \sqrt{Z_0}(\mathbf{I} + \mathbf{\Gamma}_\mathrm{L})\mathbf{a}_\mathrm{L}, \quad (3.20)$$

where the relationship in (3.18b) was used. Inserting (3.13) and (3.19) into (3.20) gives the voltage on the load as a function of the open-circuit voltage on the antennas expressed as

$$\mathbf{v}_\mathrm{L} = \underbrace{\frac{1}{2}(\mathbf{I} + \mathbf{\Gamma}_\mathrm{L})\mathbf{C}_1\mathbf{C}_2(\mathbf{I} - \mathbf{S}^{(\mathrm{R})}_{\mathrm{C}})}_{\mathbf{D}_\mathrm{R}}\mathbf{v}_\mathrm{oc} + \underbrace{\sqrt{Z_0}(\mathbf{I} + \mathbf{\Gamma}_\mathrm{L})\mathbf{C}_1\mathbf{C}_3}_{\mathbf{D}^{(\mathrm{b})}_\eta}\mathbf{b}_\eta + \underbrace{\sqrt{Z_0}(\mathbf{I} + \mathbf{\Gamma}_\mathrm{L})\mathbf{C}_1}_{\mathbf{D}^{(\mathrm{a})}_\eta}\mathbf{a}_\eta, \quad (3.21)$$

where $\mathbf{D}_\mathrm{R}$ is a linear operator that converts open-circuit voltages on the antennas to voltages on the loads.

3.5 Matched Filter

The matched filter is designed to separate the signals from each transmit source that arrive at each load termination. The mathematical details of this filter are omitted due to the variations in the methods of producing orthogonal waveforms and the type of signal transmitted. The analysis in this thesis assumes that the matched filter is able to perfectly separate the transmit signals. Mathematically, by substituting (3.10) into (3.21), the contribution to the voltage on the kth load from the nth transmit source is given by

$$v_{\mathrm{L}}^{(k,n)} = \sum_{\ell}^{N_{\mathrm{R}}} \sum_{q}^{N_{\mathrm{Q}}} \sum_{m}^{N_{\mathrm{T}}} D_{\mathrm{R},k\ell} e_{\mathrm{R},\ell}(\theta_q) H_{\ell q m} \{ e_{\mathrm{T},m}(\theta_q) D_{\mathrm{T},mn} a_{\mathrm{in},n} \}, \tag{3.22}$$

where N_{R} is the number of receive antennas. This signal represents the voltage received on the virtual element defined by the nth transmit and kth receive pair. The noise terms from (3.21) are not shown to enable simple interpretation of this result in the subsequent chapter.

Chapter 4

Signal Analysis

The energy produced by the electronics of a single transmit channel is intended to propagate out of its corresponding antenna. Although this is true for the majority of the energy, coupling causes some energy intended for one antenna to transmit from other antennas. Once energy couples into another channel, we label it as a *coupled* signal. Any energy that remains in the correct channel we label as a *uncoupled* signal. Energy can couple into adjacent channels in both the transmit and receive portions of the radar.

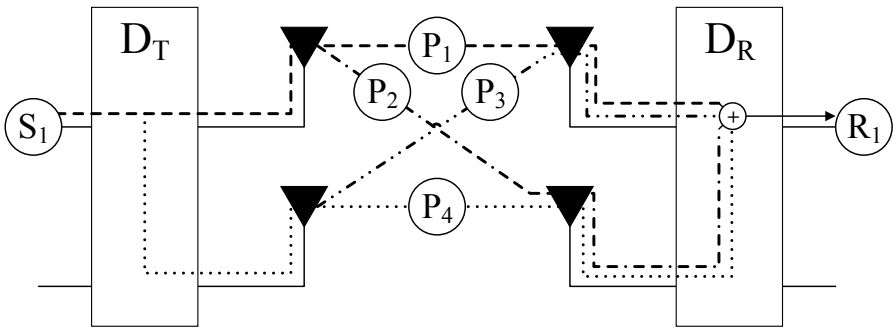

Figure 4.1: Paths followed by signals as they travel through the system.

Figure 4.1 shows the different paths that the signal can follow from the first channel of the transmit electronics to the first receive load. Section 2.3 demonstrates that each virtual element is defined by a transmit and receive antenna pair, with the received signal on the first virtual antenna element consisting of the sum of all signals that originate from the first transmit channel and arrive at the first receive load. Figure 4.1 shows that signals can follow a number of different paths and still satisfy this constraint.

To mathematically define coupled and uncoupled signals, recall that when the nth transmitter is excited the voltage at the kth load is given by (3.22) as

$$v_{\mathrm{L}}^{(k,n)} = \sum_{\ell}^{N_{\mathrm{R}}} \sum_{m}^{N_{\mathrm{T}}} D_{\mathrm{R},k\ell} e_{\mathrm{R},\ell}(\theta_q) H_{\ell q m} \{ e_{\mathrm{T},m}(\theta_q) D_{\mathrm{T},mn} a_{\mathrm{in},n} \}, \tag{4.1}$$

where the noise terms have been ignored and it is assumed that only one target is present. The indices k and ℓ indicate the receive channels while m and n indicate the transmit channel. For the example given in Fig. 4.1 with two transmit channels and two receive channels, there will be four unique combinations of transmit-receive pairs. Each of these combinations corresponds to a virtual antenna element.

As can be seen in (4.1) the signal received on each virtual antenna element is a summation of different terms, each of which has a one-to-one mapping to a unique path through the system. As an example, path 2 in Fig. 4.1 corresponds to the term

$$D_{\mathrm{R},12} e_{\mathrm{R},2}(\theta_q) H_{2q1} \{ e_{\mathrm{T},1}(\theta_q) D_{\mathrm{T},11} a_{\mathrm{in},1} \}, \tag{4.2}$$

where the signal originates on the first transmit channel ($a_{\mathrm{in},1}$), continues to the first transmit antenna ($D_{\mathrm{T},11}$), propagates through the channel from the first transmit antenna to the target and back to the second receive antenna ($H_{2q1}\{\cdot\}$), and finally couples from the second receive channel to the first ($D_{\mathrm{R},12}$). This ability to define uncoupled and coupled signals mathematically allows us to choose which signals are present when executing a simulation.

4.1 Simulation

The radar is fixed at the origin of the simulation domain, as shown in Fig. 4.2. The transmit and receive antennas are arranged in linear arrays along the horizontal axis. The S-parameter matrices $\mathbf{S}_{\mathrm{C}}^{(\mathrm{T})}$ and $\mathbf{S}_{\mathrm{C}}^{(\mathrm{R})}$ for these mutually coupled arrays are computed from the closed-form expressions for the impedance matrix of dipoles [19].

A point target is placed in the far field of the radar at the point q. This target is moved along a path where the distance between the target and the radar is the same along the entire path. The angle between the horizontal axis and the target, labeled as θ_q, is

referred to as the *target angle*. This target angle is swept along the path shown in Fig. 4.2 beginning at 0° and ending at 180°.

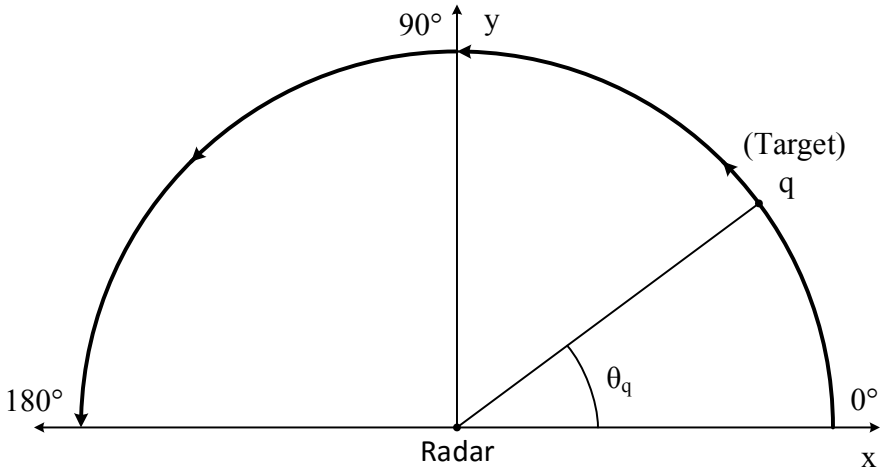

Figure 4.2: Positions of radar and target in simulation.

Simulated data is generated for each virtual element with the target at discrete positions along the path. At each position, beamforming is performed using the data from the virtual elements. Only the data corresponding to the range bin containing the target is used. For each target angle, the output of the beamformer is computed over the range $[0°, 180°]$ in 1° increments. The result is then displayed in a two-dimensional plot as a function of both target angle and beamforming angle.

The simulation is run for three different cases: only uncoupled signals present, only coupled signals present, and all signals present. Each case differs only in which signals contribute to the received signals on the virtual elements.

4.2 Uncoupled Signals

The uncoupled signal consists only of the signals that follow the path that leads directly from the transmit channel to the receive load associated with a given virtual element. An example of an uncoupled signal can be seen in Fig. 4.1 as path 1. To compute the contribution of the uncoupled signals to the given virtual element, we keep only the terms

from (4.1) that correspond to uncoupled paths. The signal received on each virtual element is

$$v_{\mathrm{L}}^{(k,n)} = D_{\mathrm{R},kk} e_{\mathrm{R},k}(\theta_q) H_{kqn} \{ e_{\mathrm{T},n}(\theta_q) D_{\mathrm{T},nn} a_{\mathrm{in},n} \}. \tag{4.3}$$

Figure 4.3 shows the result of this simulation that includes the contribution of the uncoupled signals. As expected, the strongest return occurs when the beamforming angle is equal to the target angle. This result is considered ideal and can be used as a baseline for quantifying the impact of coupling on radar system performance.

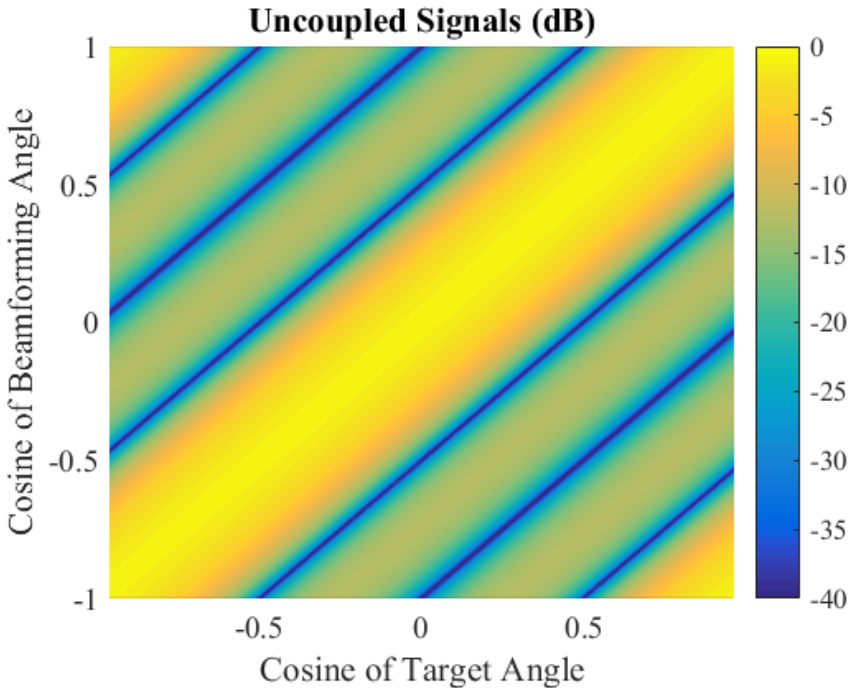

Figure 4.3: Result from the simulation as a function of target angle and beamforming angle with contributions only from the uncoupled signals.

4.3 Coupled Signals

The coupled signals consist of the remaining signals that contribute to the signal on each virtual element. Examples of coupled signals can be seen in Fig. 4.1 as paths 2, 3, and 4. In this case, we compute the contribution of the coupled signals to the given virtual

element by keeping only the terms from (4.1) that correspond to coupled paths. The signal received on each virtual element becomes

$$v_{\mathrm{L}}^{(k,n)} = \sum_{\ell,m \in P} D_{\mathrm{R},k\ell} e_{\mathrm{R},\ell}(\theta_q) H_{\ell q m} \{ e_{\mathrm{T},m}(\theta_q) D_{\mathrm{T},mn} a_{\mathrm{in},n} \}, \tag{4.4}$$

where

$$\begin{aligned} P = \{(\ell, m) : & 1 \leq \ell \leq N_{\mathrm{R}}, \\ & 1 \leq m \leq N_{\mathrm{T}}, \\ & \ell \neq k \vee m \neq n\}. \end{aligned} \tag{4.5}$$

Figure 4.4 provides the result of this simulation. Because the coupled signals do not place the strongest return at the actual target position, we anticipate that these coupled signals introduce error when they are included in the simulation.

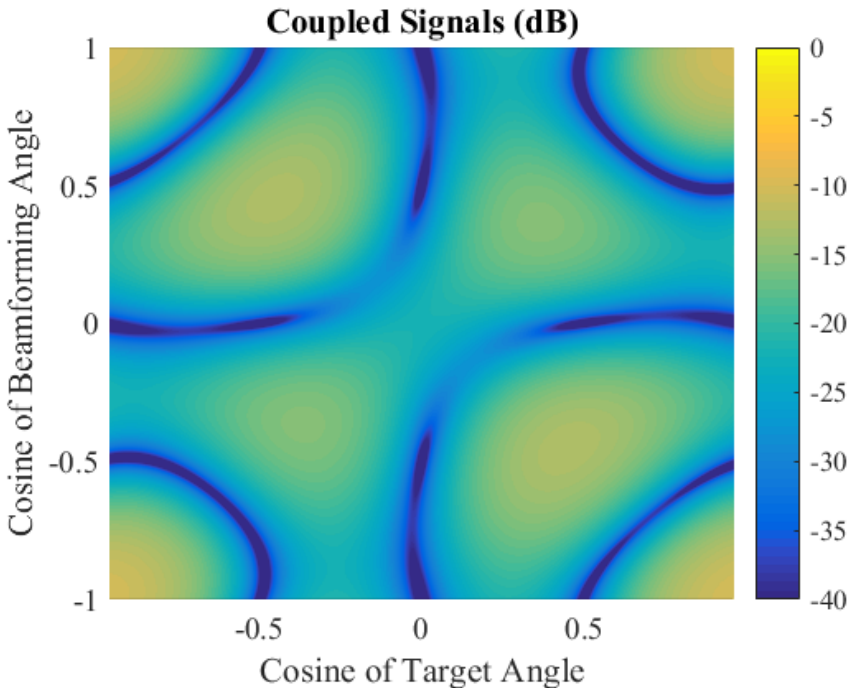

Figure 4.4: Result from the simulation as a function of target angle and beamforming angle with contributions only from the coupled signals.

4.4 All Signals

We now include both uncoupled and coupled signals to determine the distortion in the performance caused by the coupling. Figure 4.5 shows the result of this simulation. Comparing Figs. 4.3 and 4.5, we see that while the major trends are preserved despite the presence of the coupling, the coupling does create distortion in the image. The remainder of the chapter focuses on quantifying the impact of this distortion on detection performance.

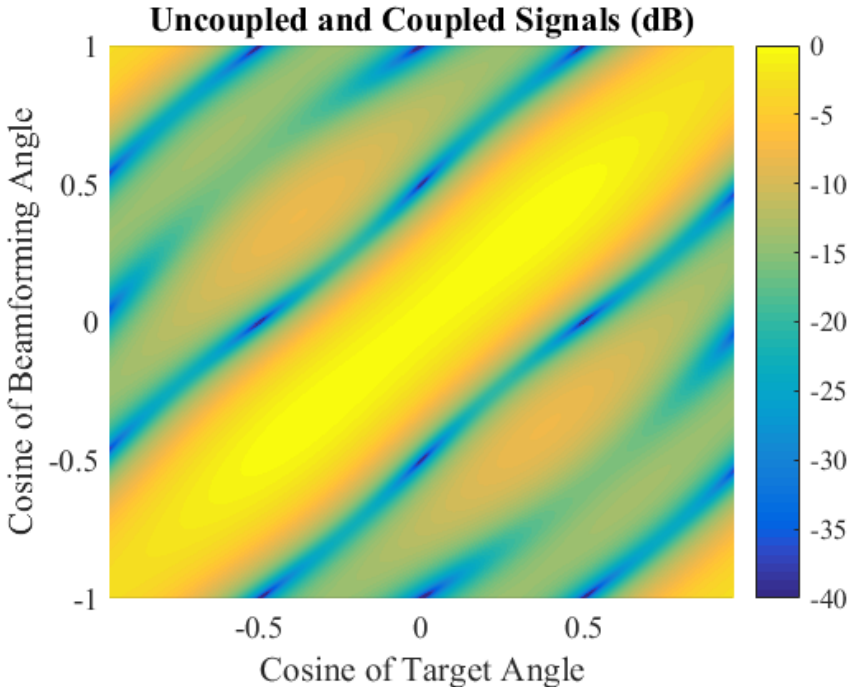

Figure 4.5: Result from the simulation as a function of target angle and beamforming angle with contributions from both the uncoupled and coupled signals.

4.5 Comparison

To highlight the impact of coupling on our simulation, we focus on the single slice from Figs. 4.3 - 4.5 at $\theta_q = \pi/4$ ($\cos(\theta_q) = 0.707$). Figure 4.6 shows these slices as a function of the beamforming angle. As can be seen from these results, coupling causes 1) the position of the peak in the beamformed signal to shift and 2) the maximum side lobe level to increase.

We therefore focus on these two phenomena to quantify the impact of coupling on MIMO radar detection performance.

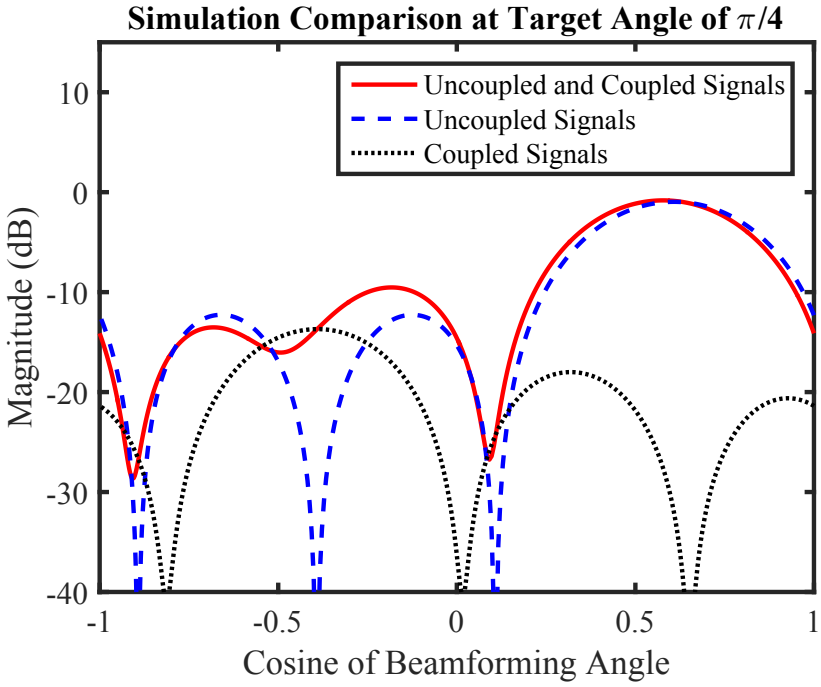

Figure 4.6: Slice from Figs. 4.3 - 4.5 when the target angle equals $\pi/4$ radians.

4.6 Target Angle Shift

The peak of the main lobe, when all signals are present, corresponds to the detected target angle, $\hat{\theta}_{\mathrm{q}}$. To automatically estimate $\hat{\theta}_{\mathrm{q}}$, we use several points near the peak of the main lobe to fit the main beam to a 4^{th}-order polynomial using least squares. $\hat{\theta}_{\mathrm{q}}$ is then the zero in the derivative of the polynomial that lies near the main beam. To test this method, we introduced known shifts into the data fed to the algorithm. The results were all within a tolerance of 0.05°, giving confidence that the angular shifts observed result from coupling rather than from the detection algorithm.

To quantify the error in the detected angle, we take the difference between the known and estimated target angles, or

$$\Delta\theta = |\theta_{\mathrm{q}} - \hat{\theta}_{\mathrm{q}}|. \tag{4.6}$$

Figure 4.7 plots $\Delta\theta$ as a function of θ_{q} for three different numbers of transmit elements (N_{T}) when $N_{\mathrm{R}} = 2$. A typical amount of coupling for an antenna array with half-wavelength spacing is used. These results show that near array broadside ($\theta_{\mathrm{q}} \approx 90°$), the impact of coupling is relatively small. However, the error caused by coupling can become quite severe as the target angle deviates from array broadside.

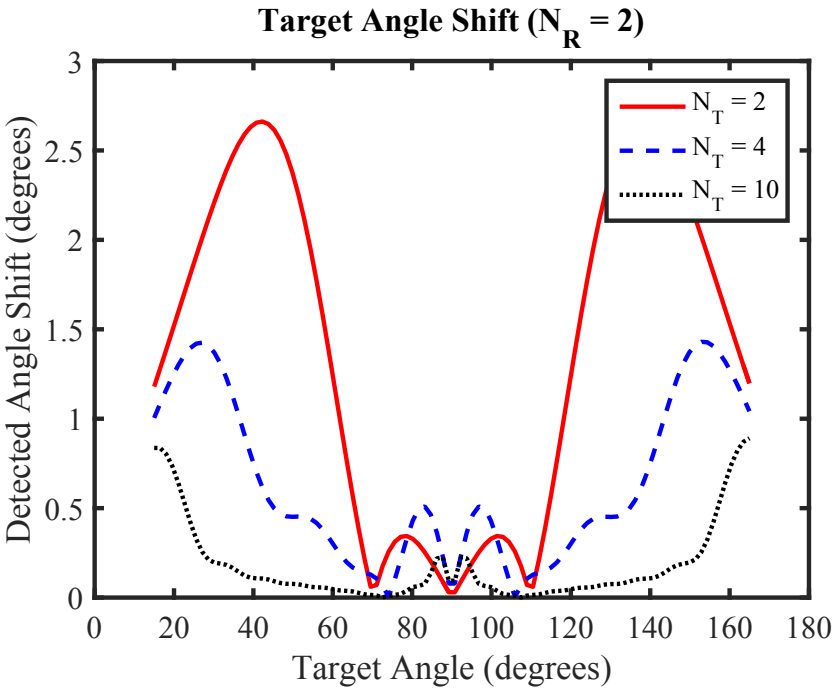

Figure 4.7: The amount the detected target angle differs from the actual target angle.

Figure 4.8 plots the maximum error $\Delta\theta$ observed over all target angles θ_{q} as a function of the coupling as measured by the value of $|S^{(\mathrm{R})}_{\mathrm{C},21}|^2$ when $N_{\mathrm{R}} = N_{\mathrm{T}} = 2$. As expected, the maximum angular shift and the coupling level are highly correlated, with strong coupling leading to severe errors in the estimated target angle.

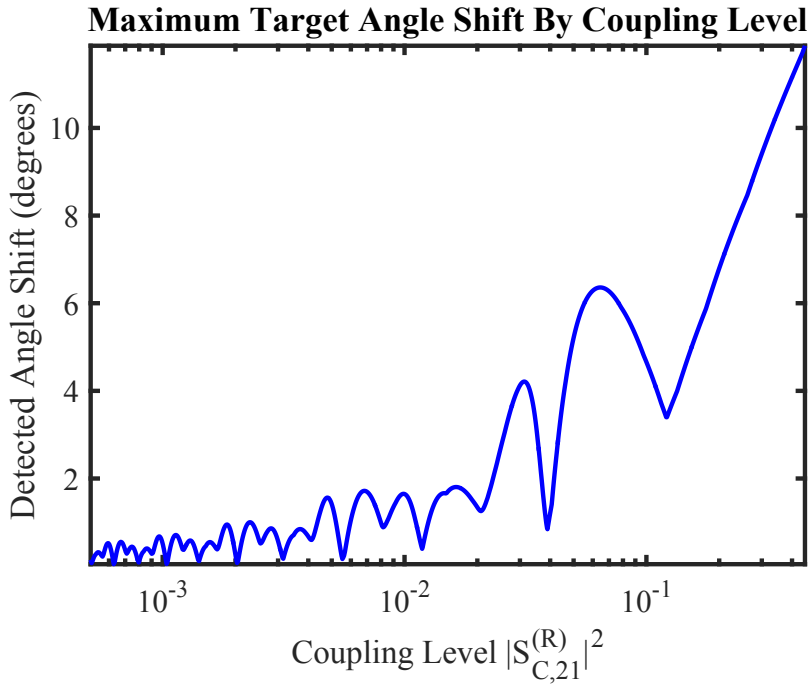

Figure 4.8: Maximum target angle shift versus coupling level.

4.7 Side Lobe Level Increase

We quantify the change ΔSLL in the side lobe level as the difference (in dB) between the peak side lobe level when all signals are present and that when only the uncoupled signals are present. Once again, this can be done for each target angle along the target path in the simulation. Figure 4.9 plots ΔSLL as a function of the target angle θ_{q} for three different values of N_{T} when $N_{\mathrm{R}} = 2$. Once again, the results show that coupling has a relatively minor impact on the side lobe level when the target is near array broadside but that the distortion can increase significantly as the target angle changes.

Figure 4.10 plots the maximum change in the side lobe level for $N_{\mathrm{R}} = N_{\mathrm{T}} = 2$ as a function of the antenna element coupling $|S_{\mathrm{C},21}^{(\mathrm{R})}|^2$. We again observe a very strong correlation between the change in the side lobe levels and the antenna array coupling.

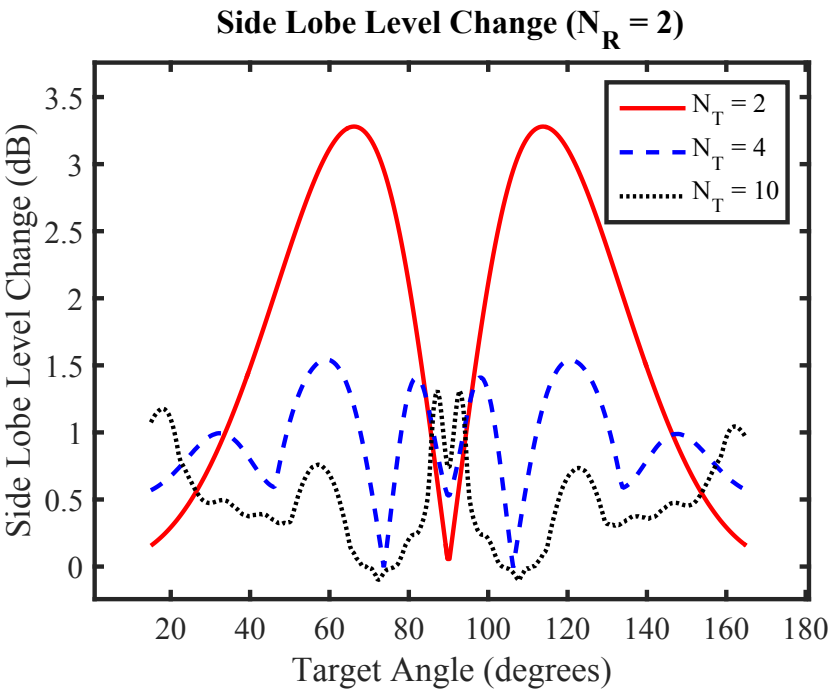

Figure 4.9: The amount the side lobe level increases for each target angle.

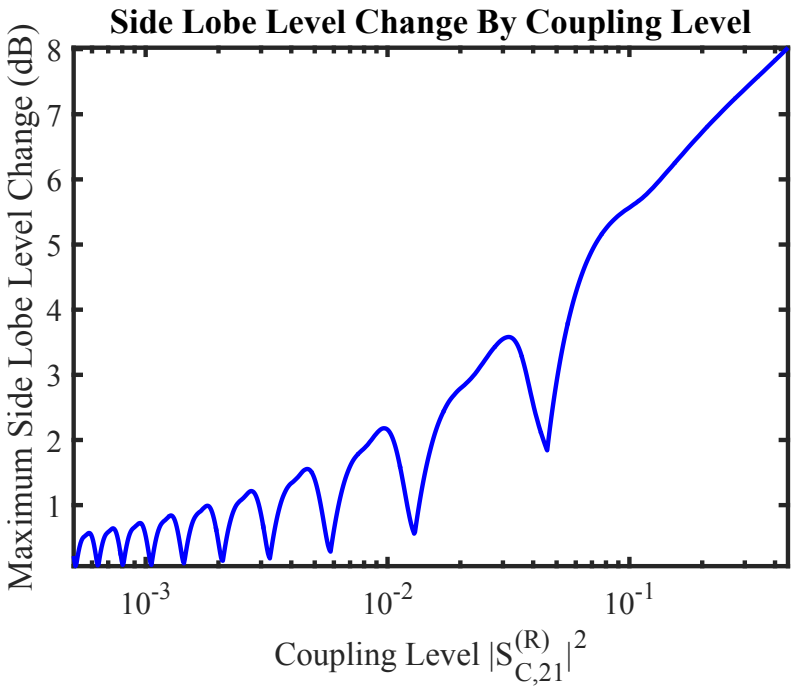

Figure 4.10: The maximum side lobe level increase versus coupling level

Chapter 5

Coupling Compensation

When the parameters of the system are accurately known then it is possible to compensate for coupling. A compensation technique to remove the effects of coupling in the transmitter and receiver is presented. The negative effects of coupling can be completely removed in controlled simulations. However, when the measurements of the system are inaccurate or when the system deviates over time from the measured values then compensating for the coupling can introduce more error than it mitigates.

5.1 Compensation Technique

The coupling in the transmitter is manifested in the system matrix $\mathbf{D}_{\mathrm{T}}$. Recall from (3.6) that the currents on the antennas are computed from the input voltages as $\mathbf{i}_2 = \mathbf{D}_{\mathrm{T}}\mathbf{a}_{\mathrm{in}}$. As long as $\mathbf{D}_{\mathrm{T}}$ is well conditioned and invertible then compensating for the transmit coupling can be acheived by computing the input voltages as

$$\mathbf{a}_{\mathrm{in}} = \mathbf{D}_{\mathrm{T}}^{-1}\mathbf{a}_{\mathrm{in,uncoupled}}, \tag{5.1}$$

where $\mathbf{a}_{\mathrm{in,uncoupled}}$ are the original input signals discussed in section 3.1.

Coupling in the receiver can be compensated for in a similar way. The system matrix $\mathbf{D}_{\mathrm{R}}$ contains all of the coupling that occurs at the receiver. It is used to compute the voltages at the loads due to open circuit voltages on the receive antennas from (3.22) as $\mathbf{v}_{\mathrm{L}}^{(n)} = \mathbf{D}_{\mathrm{R}}\mathbf{v}_{\mathrm{oc}}^{(n)}$, where the superscript n denotes the nth matched filter selecting the nth source in $\mathbf{a}_{\mathrm{in,original}}$. The matrix $\mathbf{D}_{\mathrm{R}}$ must also be well conditioned and invertible. Compensating for the coupling in the receiver is accomplished by computing new load voltages as

$$\mathbf{v}_{\mathrm{L,new}}^{(n)} = \mathbf{D}_{\mathrm{R}}^{-1}\mathbf{v}_{\mathrm{L}}^{(n)}. \tag{5.2}$$

As coupling levels increase, the matrices $\mathbf{D}_{\mathrm{T}}$ and $\mathbf{D}_{\mathrm{R}}$ can become ill conditioned and difficult to invert. The more ill conditioned these matrices become the less effective this technique is at removing the effects of coupling. However, for practical levels of coupling the matrices $\mathbf{D}_{\mathrm{T}}$ and $\mathbf{D}_{\mathrm{R}}$ remain well conditioned and are invertible.

5.2 Inaccurate Measurement

When measuring $\mathbf{D}_{\mathrm{T}}$ and $\mathbf{D}_{\mathrm{R}}$ to be used in (5.1) and (5.2) there will be inaccuracies and noise present. Modeling inaccurate measurements is accomplished by adding white Gaussian noise to the system matrices, $\mathbf{D}_{\mathrm{T}}$ and $\mathbf{D}_{\mathrm{R}}$. The measured system matrices are computed as

$$\mathbf{D}_{\mathrm{T,measured}} = \mathbf{D}_{\mathrm{T}} + \mathbf{\Psi}_{\mathrm{T}} \tag{5.3}$$

$$\mathbf{D}_{\mathrm{R,measured}} = \mathbf{D}_{\mathrm{R}} + \mathbf{\Psi}_{\mathrm{R}}, \tag{5.4}$$

where $\mathbf{\Psi}_{\mathrm{T}}$ and $\mathbf{\Psi}_{\mathrm{R}}$ are matrices with elements that are i.i.d. complex Gaussian random variables with zero-mean and variance of σ_n^2.

We now use the simulation discussed in section 4.1 to determine how much inaccurate measurements will affect the performance of the system. The number of transmit and receive antennas are both set to two and the coupling level is fixed with a typical value for dipoles at a spacing of one-half wavelength. The coupling compensation technique is applied by using (5.1) and (5.3) as the inputs to the simulation and by modifying the outputs of the simulation according to (5.2) and (5.4).

For each simulation execution new values of $\mathbf{D}_{\mathrm{T,measured}}$ and $\mathbf{D}_{\mathrm{R,measured}}$ are realized based on the statistical parameter σ_n^2. Therefore, the performance metrics from sections 4.6 and 4.7 that are computed from each simulation output will also have a statistical nature. The mean and variance of these performance metrics are estimated for a specific value of σ_n^2 by using the data from 50 simulation realizations.

Figure 5.1 plots the mean and the variance of the maximum target angle shift for different levels of the noise variance σ_n^2. The vertical axis corresponds to the maximum angle shift measured in degrees and the horizontal axis corresponds to the ratio between the noise variance and the matrix two norm of $\mathbf{D}_{\mathrm{R}}$. The mean of the error is consistently zero.

However, the variance is strongly correlated with the measurement noise ratio and becomes large as the measurement noise ratio rises above -30 dB.

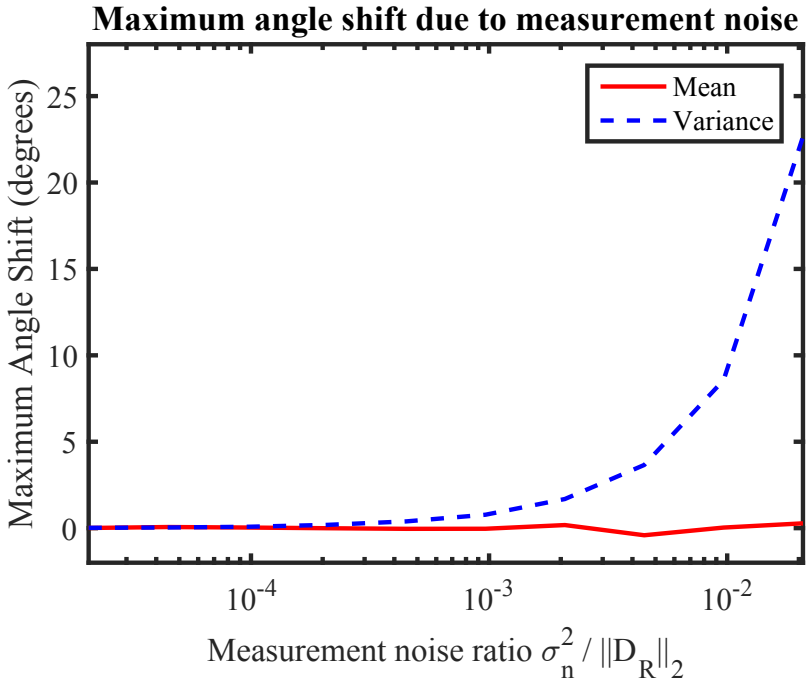

Figure 5.1: The target angle shift that occurs when noise is present in the measurements of D_{T} and D_{R}

Figures 5.2 and 5.3 are plots of the mean and variance, respectively, of ΔSLL for different levels of the noise variance σ_n^2. The vertical axis in each plot corresponds to the maximum ΔSLL that occurs and the horizontal axis in each plot corresponds to the ratio between the noise variance and the matrix two norm of $\mathbf{D}_{\mathrm{R}}$. The mean of ΔSLL has a strong correlation with the measurement noise ratio and is large for small amounts of noise. The variance also has a strong correlation with the measurement noise ratio but is relatively small.

If the inaccuracy in the measurements of $\mathbf{D}_{\mathrm{T}}$ and $\mathbf{D}_{\mathrm{R}}$ is large enough then compensating for the coupling actually makes the performance worse.

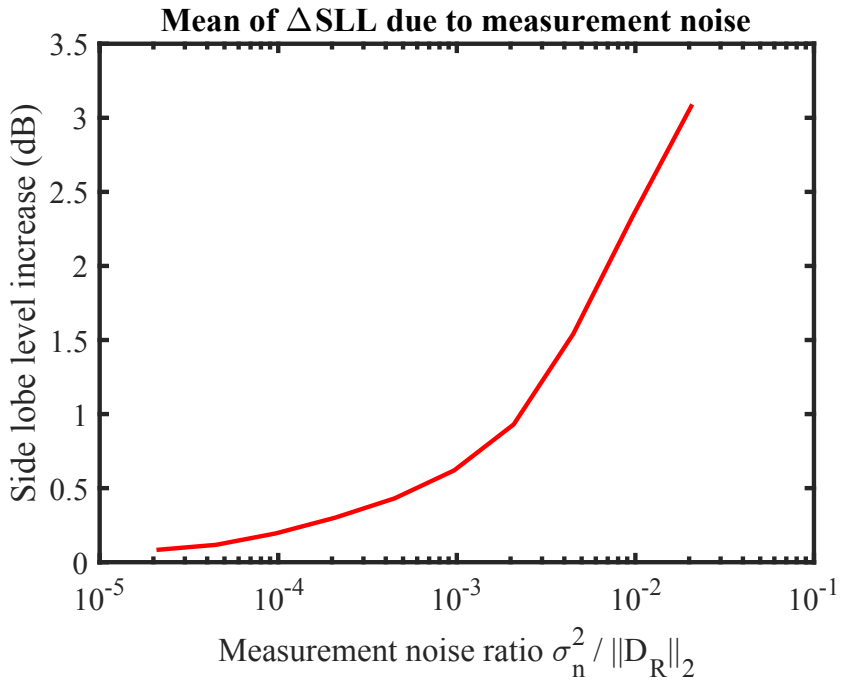

Figure 5.2: The mean of ΔSLL that occurs when noise is present in the measurements of D_{T} and D_{R}

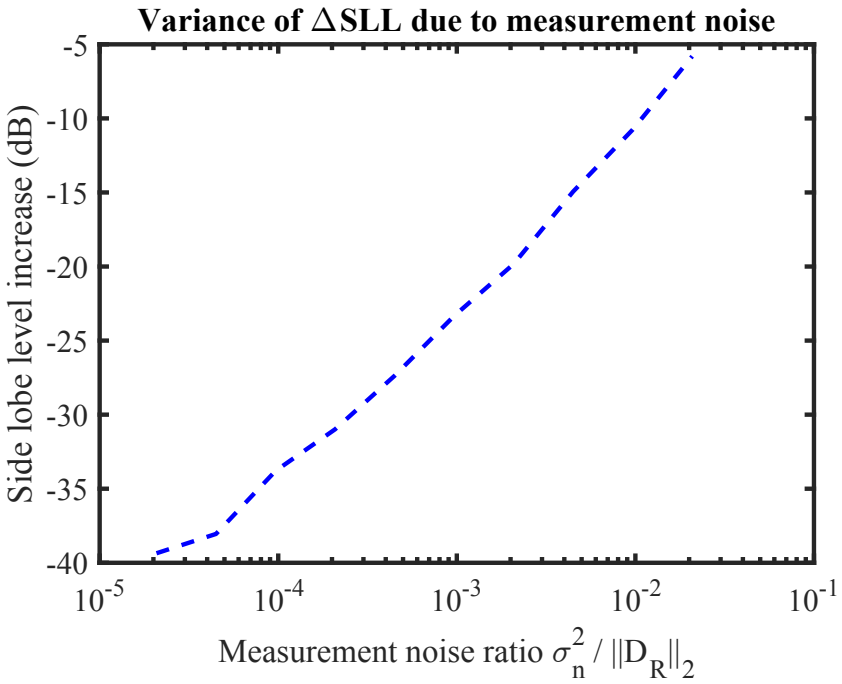

Figure 5.3: The variance of ΔSLL that occurs when noise is present in the measurements of D_{T} and D_{R}

5.3 Time-Varying Components

Over time, individual component properties change due to the environment, temperature, and use. This change introduces independent phase shifts on each transmit and receive port. Modeling these time-varying components is accomplished by computing new system matrices to replace $\mathbf{D}_{\mathrm{T}}$ and $\mathbf{D}_{\mathrm{R}}$ and are computed as

$$\mathbf{D}_{\mathrm{T,new}} = \mathbf{A}_{\mathrm{T,left}}\mathbf{D}_{\mathrm{T}}\mathbf{A}_{\mathrm{T,right}} \tag{5.5}$$

$$\mathbf{D}_{\mathrm{R,new}} = \mathbf{A}_{\mathrm{R,left}}\mathbf{D}_{\mathrm{R}}\mathbf{A}_{\mathrm{R,right}}, \tag{5.6}$$

where each $\mathbf{A}$ matrix is diagonal with elements $A_{nn} = e^{j\phi_n}$ introducing an indepedent phase shift ϕ_n distributed i.i.d. with zero-mean and a variance of σ_p^2.

The same simulations described in section 5.2 are used here. However, it is assumed that the system matrices $\mathbf{D}_{\mathrm{T}}$ and $\mathbf{D}_{\mathrm{R}}$ were measured perfectly but the actual system matrices change over time according to (5.5) and (5.6).

For each simulation execution new system matrices are realized according to (5.5) and (5.6) characterized by the parameter σ_p^2. Again, the mean and variance of the performance metrics described in sections 4.6 and 4.7 are estimated for a specific value of σ_p^2 by using the data from 50 simulation realizations.

Figure 5.4 plots the mean and the variance of the maximum target angle shift for different levels of the phase variance σ_p^2. The mean of the error is consistently zero. However, the variance is strongly correlated with the phase variance and is large when the phase variance becomes larger than 10^{-2} radians or about 0.5 degrees.

Figures 5.5 and 5.6 are plots of the mean and variance, respectively, of ΔSLL for different levels of the phase variance σ_p^2. The mean and variance of ΔSLL have a strong correlation with the phase variance.

These results suggest that the coupling compensation technique described here is highly sensitive to phase changes in time-varying components. Even small amounts of phase variance are enough to cause the performance of the system to be worse when compensating for the coupling.

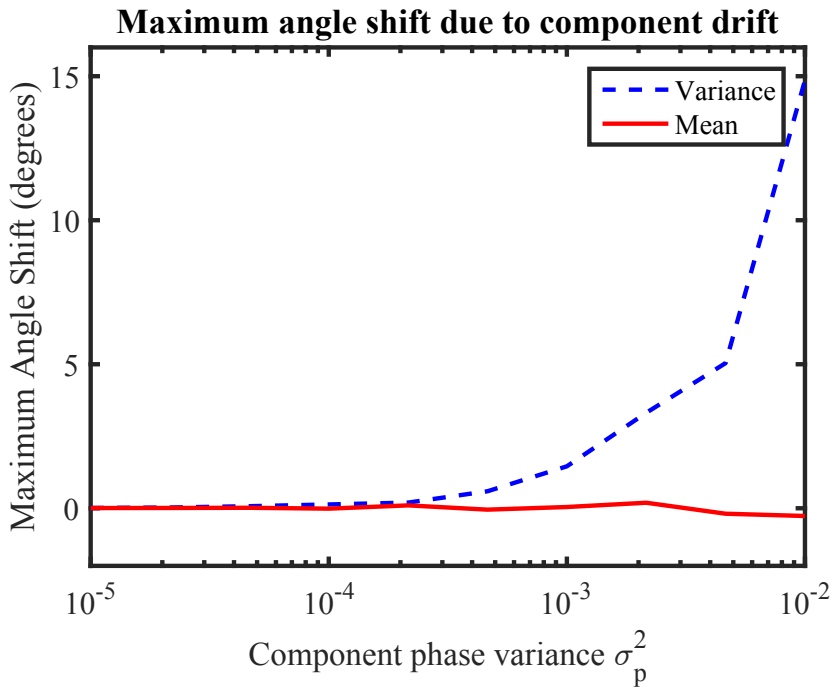

Figure 5.4: The target angle shift that occurs when the system components are time-varying

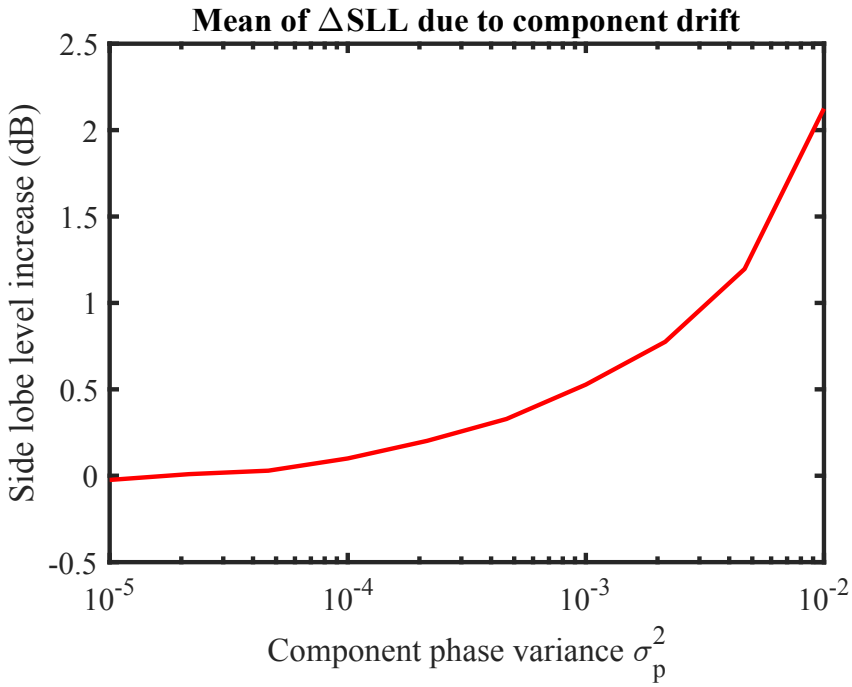

Figure 5.5: The mean of ΔSLL that occurs when the system components are time-varying

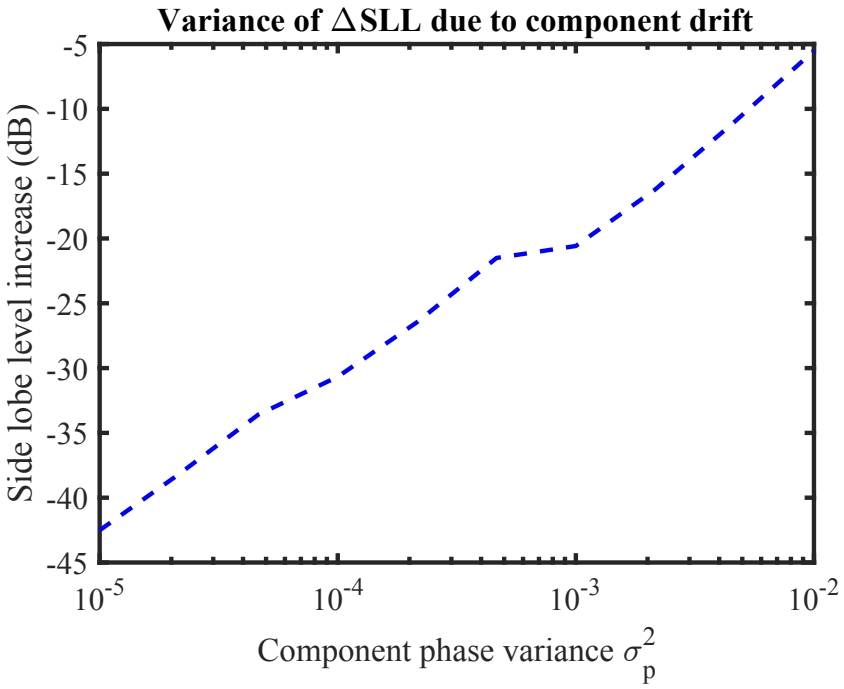

Figure 5.6: The variance of ΔSLL that occurs when the system components are time-varying

Chapter 6

Impedance Matching

Here, we consider different matching network design criteria and their impact on performance. We focus attention on impedance matching techniques that have been applied to MIMO communications systems [8–10, 21]. Because the details of these designs have already been well documented, only a high level description will be given here.

A well designed matching network maximizes the power transfer from a source to a load. For the transmit portion of the radar, the objective is to match the transmit electronics to the coupled transmit antennas. Similarly, at the receiver, the objective is to match the coupled receive antennas to the receive electronics. We use the diagram in Fig. 6.1 to represent both of these scenarios to facilitate the discussion.

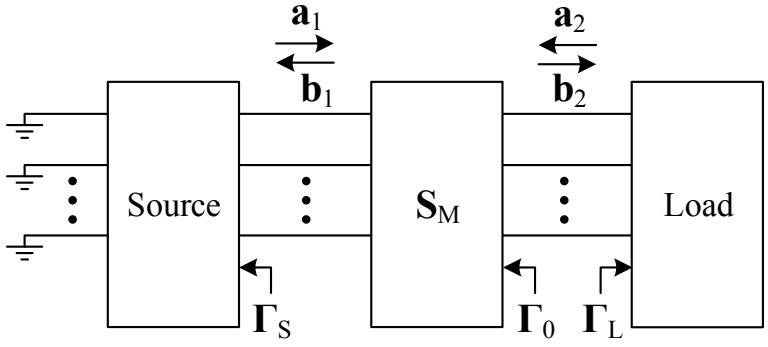

Figure 6.1: Matching Network Diagram.

Matching network design involves determining the S-parameters of the matching network such that $\mathbf{\Gamma}_S$ is transformed to a desired value of $\mathbf{\Gamma}_0$. For example, optimal matching produces $\mathbf{\Gamma}_0 = \mathbf{\Gamma}_L^H$, where $\{\cdot\}^H$ is a conjugate transpose. Alternatively, different techniques

can be used to approximate the criterion $\mathbf{\Gamma}_0 = \mathbf{\Gamma}_{\mathrm{L}}^{\mathrm{H}}$ under different simplifying assumptions. Once $\mathbf{\Gamma}_0$ has been chosen, the network S-parameters can be established using a technique based on the singular value decomposition as detailed in [13] and summarized in Appendix A.

6.1 Matching Criteria

Choosing $\mathbf{\Gamma}_0$ to have non-zero off-diagonal elements causes the matching network S-parameter matrix to also be full. While this can give optimal performance, such a matching network tends to be difficult to build and is typically very narrow band [9]. Since radars often use a large bandwidth, this coupled matching network is impractical. We therefore limit the S-parameter matrix of the matching network to consist of blocks that are diagonal matrices which means that the input and output ports are paired [10], [11] (no coupling among multiple ports).

We consider three different criteria for matching network design under this constraint: self impedance, input impedance, and active impedance. The criteria differ only in how a diagonal reflection coefficient matrix $\mathbf{\Gamma}_0$ is computed from the full coupled reflection coefficient matrix $\mathbf{\Gamma}_{\mathrm{L}}$. In the following, we use the impedance matrix $\mathbf{Z}_{\mathrm{L}}$ to correspond to the reflection coefficient $\mathbf{\Gamma}_{\mathrm{L}}$.

6.1.1 Self Impedance

The self impedance match is realized by forming the diagonal matrix $\mathbf{Z}_{\mathrm{L}}^{(\mathrm{D})}$ consisting of the diagonal elements of $\mathbf{Z}_{\mathrm{L}}$ and then forming the reflection coefficient $\mathbf{\Gamma}_{\mathrm{L}}^{(\mathrm{D})}$ from $\mathbf{Z}_{\mathrm{L}}^{(\mathrm{D})}$ [22]. We then use $\mathbf{\Gamma}_0 = \mathbf{\Gamma}_{\mathrm{L}}^{(\mathrm{D})*}$ in our network design technique.

6.1.2 Input Impedance

The input impedance match finds the reflection coefficient $\mathbf{\Gamma}_{\mathrm{L},i}^{(\mathrm{in})}$ looking into the ith load port when all other ports of the load are terminated. Forming the diagonal matrix $\mathbf{\Gamma}_{\mathrm{L}}^{(\mathrm{in})}$ whose ith diagonal element is $\mathbf{\Gamma}_{\mathrm{L},i}^{(\mathrm{in})}$, the objective is to find the diagonal matrix $\mathbf{\Gamma}_0$ such that $\mathbf{\Gamma}_0 = \mathbf{\Gamma}_{\mathrm{L}}^{(\mathrm{in})*}$. Since $\mathbf{\Gamma}_{\mathrm{L}}^{(\mathrm{in})}$ depends on $\mathbf{\Gamma}_0$, this is typically computed iteratively [23].

6.1.3 Active Impedance

The active impedance matrix $\mathbf{Z}_{\text{act}}$ is a diagonal matrix with the objective of maintaining the voltages and currents obtained from an optimal conjugate impedance match for a specified incident field. The reflection coefficient $\mathbf{\Gamma}_{\text{act}}$ is formed from the active impedance matrix $\mathbf{Z}_{\text{act}}$. The active impedance match, $\mathbf{\Gamma}_0 = \mathbf{\Gamma}_{\text{act}}^*$, achieves maximum power transfer for the designated incident field but power transfer is suboptimal for any other incident field [18].

More commonly, a range of incident fields are present. Achieving maximum power transfer simultaneously for every incident field is not possible when using uncoupled terminations. However, the uncoupled solution $\mathbf{Z}_{\text{L}}^{(\text{act})}$ can be found such that the performance on average is optimized. Typically this solution is found iteratively. The reflection coefficicient is then formed from $\mathbf{Z}_{\text{L}}^{(\text{act})}$ as $\mathbf{\Gamma}_{\text{L}}^{(\text{act})}$ and is used in designing the network [23].

6.2 Performance

We now examine how these matching network design criteria affect the target angle shift and the side lobe level increase introduced in chapter 4. We again consider a system with $N_{\text{R}} = N_{\text{T}} = 2$, and we run this simulation for no matching network as well as self impedance, input impedance, and active impedance matching networks.

6.2.1 Target Angle Shift

Figure 6.2 plots the error $\Delta\theta$ in the estimated target area as a function of the actual target angle θ_{q}. As can be seen, all three matching networks can dramatically reduce the error for most target angles.

Figure 6.3 plots the maximum observed $\Delta\theta$ as a function of the amount of coupling in the transmit and receive arrays. These results show that as the coupling gets large, trying to design an approximate matching network (input impedance match) can underperform removal of the matching network. For practical levels of coupling the performance is not greatly impacted by the choice of matching network criteria as the results may be better or worse depending on the coupling level.

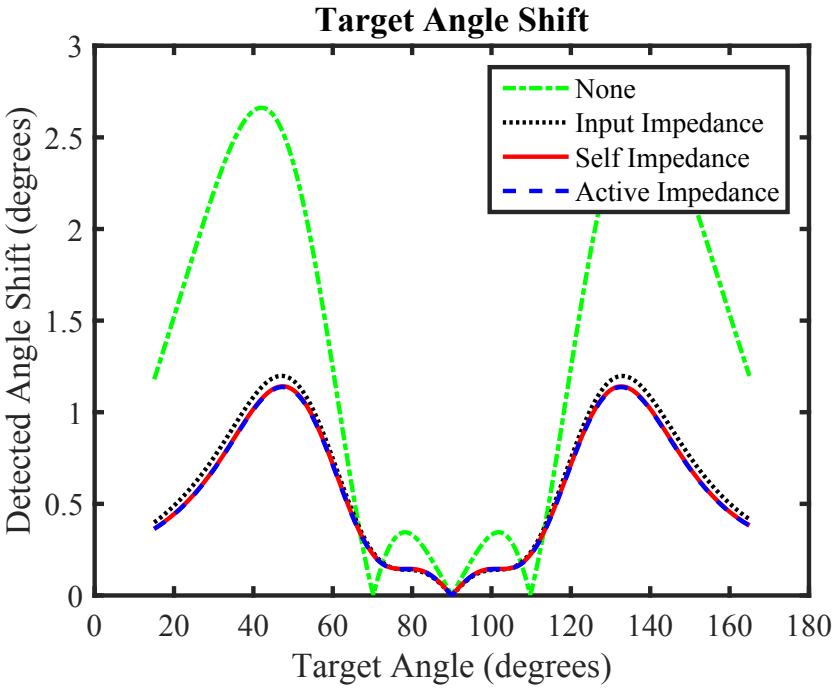

Figure 6.2: The amount the detected target angle differs from the actual target angle for different impedance matching criteria.

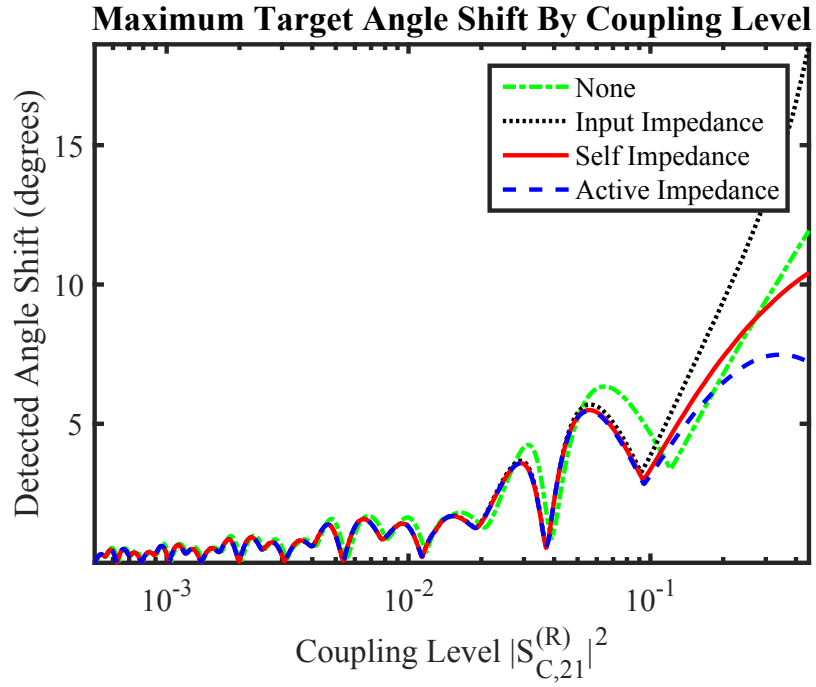

Figure 6.3: Maximum target angle shift versus coupling level for different impedance matching criteria.

6.2.2 Side Lobe Level Increase

Figure 6.4 plots the increase ΔSLL in the side lobe level as a function of the target angle θ_q for the different impedance matching designs. The results again demonstrate that there can be improvement when impedance matching is included.

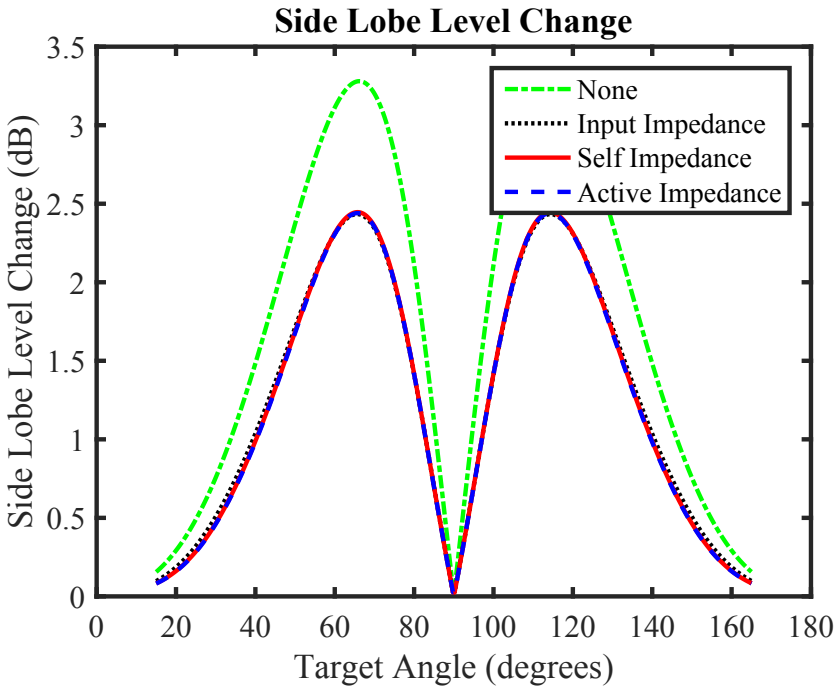

Figure 6.4: The increase in side lobe level for different impedance matching criteria.

Figure 6.5 plots the maximum value of ΔSLL as a function of the level of coupling, again confirming that at high coupling, the active impedance match offers the best overall performance. However, for practical levels of coupling the choice of impedance matching criteria does not have a significant impact on performance.

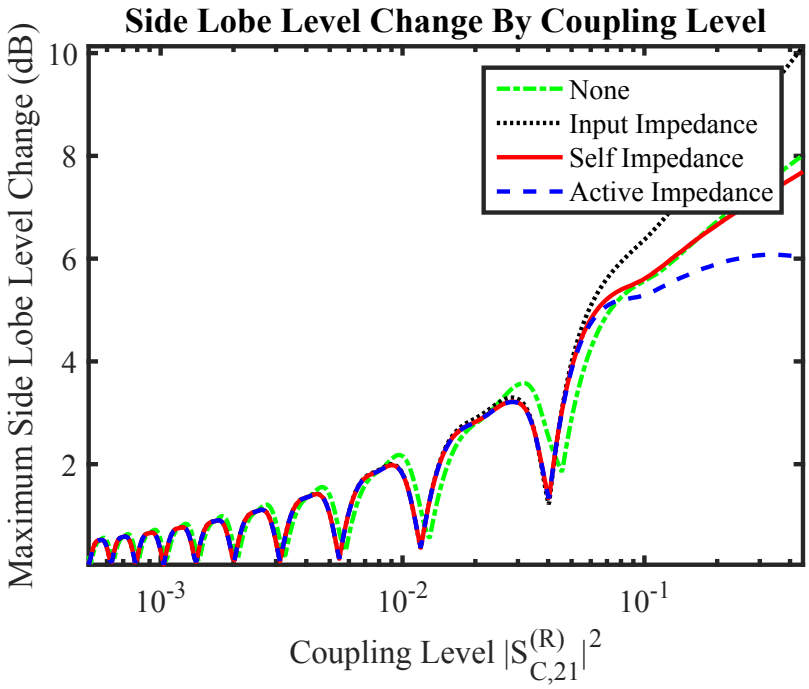

Figure 6.5: The maximum increase in side lobe level versus coupling level for different impedance matching criteria.

Chapter 7

Conclusion

This thesis presents a detailed model of a MIMO radar system that includes transmit and receive electronics, coupled antenna arrays, and a target response. The system model analysis uses network theory to represent the signals as they travel through the system. These signals are designated as either uncoupled or coupled signals in order to assess the impact that coupling has on the radar performance.

Simulations based on the model demonstrate that mutual coupling can have a significant detrimental impact on the performance of a MIMO radar. The results show that both the accuracy of the estimated target angle as well as the level of the side lobes associated with the target beamforming are affected. Depending on the application, even a normal level of coupling can shift the perceived target angle or increase the side lobe level enough to cause inaccurate results.

The compensation technique presented in chapter 5 can completely remove the negative effects of coupling for practical systems. However, simulated results showed that when the system is not measured properly or the system changes over time the compensation technique presented will introduce more error rather than removing it.

The thesis also illustrates the impact of impedance matching design on the achieved performance. The results show that while the impacts of coupling cannot be completely removed through practical impedance matching, good designs may improve performance depending on the coupling level.

7.1 Future Work

While this thesis offers a significant advancement in the analysis of MIMO radar systems with mutual coupling, additional work in the future could further advance our understanding on this area.

- In addition to the metrics proposed here, it is possible to explore how the 3 dB angular width of a target is affected by coupling in the system. Accomplishing this requires decoupling the change in the 3 dB angular width from the change in angular width caused by the angular shift as the target moves to different angles. Furthermore, only one type of antenna layout was tested in this thesis. Further arrangements, including circular or square arrays, could be tested.

- The system model presented in chapter 3 does not take into consideration coupling that will occur between transmit and receive antennas. This connection was not included in this thesis due to the complexity added to the mathematical model but could be considered as future work.

- Further matching network design techniques could be considered. When the scattering parameters of a matching network are coupled the network usually has narrow operating bandwidth. The constraints from needing higher bandwidth on the scattering parameters could be explored. Perhaps some coupling can be allowed in the matching network. However, the design of the matching network is more complicated than simply achieving maximum power transfer. The majority of the energy for a given transmit channel needs to be transmitted from its associated transmit antenna.

- Additional research could be done allowing the transmit and receive matching networks to be connected. This could help compensate for some of the coupling that occurs between the transmit and receive antennas which was not discussed in this thesis.

- It may be possible to compensate for the transmit coupling at the receiver. This study only explored the method of compensating for the transmit coupling at the transmitter.

Appendix A

Matching Network Design

A well designed matching network optimizes the power transfer from the source to the load. Conjugate matching delivers optimal power transfer and is achieved when $\mathbf{\Gamma}_0 = \mathbf{\Gamma}_{\mathrm{L}}^H$ in Fig. A.1. The matching network, with S-parameter matrix $\mathbf{S}_{\mathrm{M}}$, is designed for known source and load reflection coefficients $\mathbf{\Gamma}_{\mathrm{S}}$ and $\mathbf{\Gamma}_{\mathrm{L}}$, respectively, to achieve a desired matching condition.

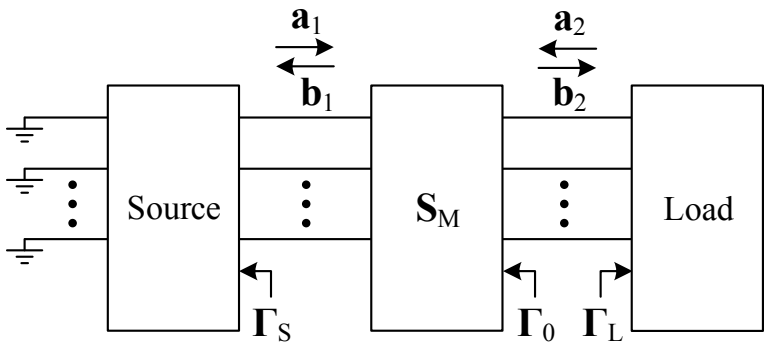

Figure A.1: Block Diagram for Matching Network Design

The matching network S-parameter matrix $\mathbf{S}_{\mathrm{M}}$ can be written as a 2×2 block matrix with elements $\mathbf{S}_{\mathrm{M},ij}$. Without any loss of generality, $\mathbf{S}_{\mathrm{M},ij}$ can be written in terms of the singular value decomposition (SVD) as

$$\mathbf{S}_{\mathrm{M},ij} = \mathbf{U}_{\mathrm{M},ij} \mathbf{\Lambda}_{\mathrm{M},ij}^{1/2} \mathbf{V}_{\mathrm{M},ij}^H, \tag{A.1}$$

where $\mathbf{U}_{\mathrm{M},ij}$ and $\mathbf{V}_{\mathrm{M},ij}$ are unitary matrices and $\mathbf{\Lambda}_{\mathrm{M},ij}^{1/2}$ is a diagonal matrix containing the singular values of $\mathbf{S}_{\mathrm{M},ij}$. Substituting (A.1) into the lossless constraint $\mathbf{S}_{\mathrm{M}}\mathbf{S}_{\mathrm{M}}^{H} = \mathbf{I}$ leads to

$$\begin{aligned}
\mathbf{S}_{\mathrm{M},11} &= \mathbf{U}_{\mathrm{M},11}\mathbf{\Lambda}_{\mathrm{M},11}^{1/2}\mathbf{V}_{\mathrm{M},11}^{H} \\
\mathbf{S}_{\mathrm{M},12} &= -\mathbf{U}_{\mathrm{M},11}\mathbf{\Theta}^{H}(\mathbf{I}-\mathbf{\Lambda}_{\mathrm{M},11})^{1/2}\mathbf{V}_{\mathrm{M},22}^{H} \\
\mathbf{S}_{\mathrm{M},21} &= \mathbf{U}_{\mathrm{M},22}\mathbf{\Theta}(\mathbf{I}-\mathbf{\Lambda}_{\mathrm{M},11})^{1/2}\mathbf{V}_{\mathrm{M},11}^{H} \\
\mathbf{S}_{\mathrm{M},22} &= \mathbf{U}_{\mathrm{M},22}\mathbf{\Lambda}_{\mathrm{M},11}^{1/2}\mathbf{V}_{\mathrm{M},22}^{H},
\end{aligned} \tag{A.2}$$

where $\mathbf{\Theta}$ is a diagonal matrix with elements that have unit magnitude and an arbitrary phase. The matching network S-parameters are now fully characterized by $\mathbf{U}_{\mathrm{M},11}$, $\mathbf{\Lambda}_{\mathrm{M},11}$, $\mathbf{V}_{\mathrm{M},11}$, $\mathbf{U}_{\mathrm{M},22}$, $\mathbf{V}_{\mathrm{M},22}$, and $\mathbf{\Theta}$.

Equations for the forward and reverse traveling waves at the port between the source and the matching network and the port between the matching network and the load from Fig. A.1 can be written as

$$\mathbf{a}_1 = \mathbf{\Gamma}_{\mathrm{S}}\mathbf{b}_1 \tag{A.3a}$$

$$\mathbf{b}_1 = \mathbf{S}_{\mathrm{M},11},\mathbf{a}_1 + \mathbf{S}_{\mathrm{M},12}\mathbf{a}_2 \tag{A.3b}$$

$$\mathbf{a}_2 = \mathbf{\Gamma}_{\mathrm{L}}\mathbf{b}_2 \tag{A.3c}$$

$$\mathbf{b}_2 = \mathbf{S}_{\mathrm{M},21}\mathbf{a}_1 + \mathbf{S}_{\mathrm{M},22}\mathbf{a}_2. \tag{A.3d}$$

Solving for $\mathbf{b}_2$ from (A.3a - A.3d) gives

$$\mathbf{b}_2 = \underbrace{\left[\mathbf{S}_{\mathrm{M},22} + \mathbf{S}_{\mathrm{M},21}(\mathbf{I}-\mathbf{\Gamma}_{\mathrm{S}}\mathbf{S}_{\mathrm{M},11})^{-1}\mathbf{\Gamma}_{\mathrm{S}}\mathbf{S}_{\mathrm{M},12}\right]}_{\mathbf{\Gamma}_0}\mathbf{a}_2. \tag{A.4}$$

Substituting the matching network S-parameters from (A.2) into (A.4) leads to

$$\mathbf{\Gamma}_0 = \mathbf{U}_{\mathrm{M},22}\underbrace{\left[\mathbf{\Lambda}_{\mathrm{M},11}^{1/2} - (\mathbf{I}-\mathbf{\Lambda}_{\mathrm{M},11})^{1/2}\mathbf{T}(\mathbf{I}-\Lambda_{\mathrm{M},11})^{1/2}\right]}_{\mathbf{B}}\mathbf{V}_{\mathrm{M},22}^{H} \tag{A.5}$$

$$\mathbf{T} = \mathbf{\Theta}\mathbf{V}_{\mathrm{M},11}^{H}(\mathbf{I}-\mathbf{\Gamma}_{\mathrm{S}}\mathbf{U}_{\mathrm{M},11}\mathbf{\Lambda}_{\mathrm{M},11}^{1/2}\mathbf{V}_{\mathrm{M},11}^{H})^{-1}\mathbf{\Gamma}_{\mathrm{S}}\mathbf{U}_{\mathrm{M},11}\mathbf{\Theta}^{H}. \tag{A.6}$$

Using the SVD $\mathbf{\Gamma}_{\mathrm{S}} = \mathbf{U}_{\mathrm{S}}\mathbf{\Lambda}_{\mathrm{S}}^{1/2}\mathbf{V}_{\mathrm{S}}^{H}$ and the substitutions $\mathbf{U}_{\mathrm{M},11} = \mathbf{V}_{\mathrm{S}}$ and $\mathbf{V}_{\mathrm{M},11} = \mathbf{U}_{\mathrm{S}}$, $\mathbf{T}$ becomes diagonal in the form

$$\mathbf{T} = (\mathbf{I} - \mathbf{\Lambda}_{\mathrm{S}}^{1/2}\mathbf{\Lambda}_{11}^{1/2})^{-1}\mathbf{\Lambda}_{\mathrm{S}}^{1/2}. \tag{A.7}$$

The matrix $\mathbf{B}$ therefore also becomes diagonal. It is then natural to say from (A.5) and $\mathbf{\Gamma}_0 = \mathbf{U}_0\mathbf{\Lambda}_0^{1/2}\mathbf{V}_0^{H}$ that $\mathbf{U}_{\mathrm{M},22} = \mathbf{U}_0$, $\mathbf{V}_{\mathrm{M},22} = \mathbf{V}_0$, and $\mathbf{B} = \mathbf{\Lambda}_0^{1/2}$ which leads to

$$\mathbf{\Lambda}_{\mathrm{M},11}^{1/2} = (\mathbf{\Lambda}_0^{1/2} + \mathbf{\Lambda}_{\mathrm{S}}^{1/2})(\mathbf{I} + \mathbf{\Lambda}_0^{1/2}\mathbf{\Lambda}_{\mathrm{S}}^{1/2})^{-1}. \tag{A.8}$$

The final solutions for the S-parameters of the matching network that achieve optimal power transfer are [13]

$$\begin{aligned}
\mathbf{S}_{\mathrm{M},11} &= \mathbf{V}_{\mathrm{S}}\mathbf{\Lambda}_{\mathrm{M},11}^{1/2}\mathbf{U}_{\mathrm{S}}^{H} \\
\mathbf{S}_{\mathrm{M},12} &= -\mathbf{V}_{\mathrm{S}}\mathbf{\Theta}^{H}(\mathbf{I} - \mathbf{\Lambda}_{\mathrm{M},11})^{1/2}\mathbf{V}_0^{H} \\
\mathbf{S}_{\mathrm{M},21} &= \mathbf{U}_0\mathbf{\Theta}(\mathbf{I} - \mathbf{\Lambda}_{\mathrm{M},11})^{1/2}\mathbf{U}_{\mathrm{S}}^{H} \\
\mathbf{S}_{\mathrm{M},22} &= \mathbf{U}_0\mathbf{\Lambda}_{\mathrm{M},11}^{1/2}\mathbf{V}_0^{H},
\end{aligned} \tag{A.9}$$

where $\mathbf{\Lambda}_{\mathrm{M},11}^{1/2}$ from (A.8) should be substituted into (A.9).

Bibliography

[1] R. Feger, C. Wagner, S. Schuster, S. Scheiblhofer, H. Jäger, and A. Stelzer, "A 77-GHz FMCW MIMO radar based on an sige single-chip transceiver," *IEEE Transactions on Microwave Theory and Techniques*, vol. 57, no. 5, pp. 1020–1035, May 2009. 1

[2] B. Friedlander, "On the relationship between MIMO and SIMO radars," *IEEE Transactions on Signal Processing*, vol. 57, no. 1, pp. 394–398, Jan. 2009. 1

[3] F. C. Robey, S. Coutts, D. Weikle, J. C. McHarg, and K. Cuomo, "MIMO radar theory and experimental results," *Signals, Systems and Computers, 2004. Conference Record of the Thirty-Eighth Asilomar Conference on*, vol. 1, pp. 300–304, Nov. 2004. 1

[4] C. Pfeffer, R. Feger, C. M. Schmid, C. Wagner, and A. Stelzer, "An IQ-modulator based heterodyne 77-GHz FMCW colocated MIMO radar system," *Microwave Symposium Digest (MTT), 2012 IEEE MTT-S International*, pp. 1–3, Jun. 2012. 1, 6

[5] Y. Huang and P. V. Brennan, "FMCW based MIMO imaging radar for maritime navigation," *Progress in electromagnetics research*, vol. 115, pp. 327–342, Apr. 2011. 1, 5, 6

[6] J. Li, P. Stoica, L. Xu, and W. Roberts, "On parameter identifiability of MIMO radar," *IEEE Signal Processing Letters*, vol. 14, no. 12, pp. 968–971, Dec. 2007. 1

[7] G. Babur, P. J. Aubry, and F. L. Chevalier, "Antenna coupling effects for space-time radar waveforms: Analysis and calibration," *IEEE Transactions on Antennas and Propagation*, vol. 62, no. 5, pp. 2572–2586, May 2014. 1

[8] K. Warnick, E. Woestenburg, L. Belostotski, and P. Russer, "Minimizing the noise penalty due to mutual coupling for a receiving array," *IEEE Trans. Antennas Propag.*, vol. 57, no. 6, pp. 1634–1644, Jun. 2009. 1, 37

[9] B. K. Lau, J. B. Andersen, G. Kristensson, and A. Molisch, "Impact of matching network on bandwidth of compact antenna arrays," *IEEE Trans. Antennas Propag.*, vol. 54, no. 11, pp. 3225–3238, Nov. 2006. 1, 37, 38

[10] B. K. Lau, J. B. Andersen, G. Kristensson, and A. F. Molisch, "Antenna matching for capacity maximization in compact MIMO systems," in *Proc. 3rd Int. Symp. Wireless Commun. Syst.*, Valencia, Spain, Sep. 2006, pp. 253–257. 1, 37, 38

[11] Y. Fei, Y. Fan, B. K. Lau, and J. Thompson, "Optimal single-port matching impedance for capacity maximization in compact MIMO arrays," *IEEE Trans. Antennas Propag.*, vol. 56, no. 11, pp. 3566–3575, Nov. 2008. 1, 38

[12] J. W. Wallace and M. A. Jensen, "Mutual coupling in MIMO wireless systems: A rigorous network theory analysis," *IEEE Trans. Wireless Commun.*, vol. 3, pp. 1317–1325, Jul. 2004. 1

[13] M. L. Morris and M. A. Jensen, "Network model for MIMO systems with coupled antennas and noisy amplifiers," *IEEE Trans. Antennas Propag.*, vol. 53, pp. 545–552, Jan. 2005. 1, 13, 38, 47

[14] L. Schumacher, K. I. Pedersen, and P. E. Mogensen, "From antenna spacings to theoretical capacities - guidelines for simulating MIMO systems," in *Proc. 2002 IEEE 13th Intl. Symp. on Personal, Indoor and Mobile Radio Comm.*, vol. 2, Lisboa, Portugal, Sep. 15-18, 2002, pp. 587–592. 1

[15] B. T. Quist and M. A. Jensen, "Optimal antenna radiation characteristics for diversity and MIMO systems," *IEEE Trans. Antennas Propag.*, vol. 57, no. 11, pp. 3474–3481, Nov. 2009. 1

[16] H. Özcelik, M. Herdin, W. Weichselberger, J. W. Wallace, and E. Bonek, "Deficiencies of 'Kronecker' MIMO radio channel model," *Electronics Letters*, vol. 39, pp. 1209–1210, Aug. 7 2003. 1

[17] S. M. Makarov, *Antenna and EM Modeling with MATLAB.* New York: John Wiley and Sons, 2002. 5, 12

[18] P. W. Hannan, "The element-gain paradox for a phased-array antenna," *IEEE Trans. Antennas Propag.*, vol. 12, no. 4, pp. 423–433, Jul. 1964. 12, 39

[19] C. A. Balanis, *Antenna Theory: Analysis and Design.* Wiley, 1997. 12, 16, 21

[20] H. A. Haus and R. B. Adler, *Circuit Theory of Linear Noisy Networks.* New York: Wiley, 1959. 17

[21] J. B. Andersen and H. H. Rasmussen, "Decoupling and descattering networks for antennas," *IEEE Trans. Antennas Propag.*, vol. AP-24, no. 6, pp. 841–846, Nov. 1976. 37

[22] K. F. Warnick and M. A. Jensen, "Effects of mutual coupling on interference mitigation with a focal plane array," *IEEE Trans. Antennas Propag.*, vol. 53, pp. 2490–2498, Aug. 2005. 38

[23] M. A. Jensen and B. K. Lau, "Uncoupled matching for active and passive impedances of coupled arrays in MIMO systems," *IEEE Trans. Antennas Propag.*, vol. 58, no. 10, pp. 3336–3343, Oct. 2010. 38, 39